(2)

Field Emission Cathode and Vacuum Microelectronic Microwave Amplifier Development

TECHNICAL PROGRESS REPORT

for the period
1 July 1992 - 31 March 1993

Submitted to

Dr. Bertram Hui
DARPA/DSO
3701 N. Fairfax Drive
Arlington, VA 22203
703/696-2239

by

Georgia Tech Research Corporation
Georgia Institute of Technology
Atlanta, Georgia 30332-0245

Principal Investigators

Dr. Wayne L. Ohlinger
Tel: 404/853-9853
FAX: 404/894-5073

Dr. D. Norman Hill
Tel: 404/894-6081
FAX: 404/853-9140

I. EXECUTIVE SUMMARY

The objective of this report is to summarize progress made to date on Contract MDA-972-91-C-0034, indicate problem areas that have been addressed, outline plans for future work, and to discuss, in a realistic manner, the likelihood that the proposed work will be completed in a reasonable time frame. There is no single, overriding reason that the project fell behind the program schedule; rather, an accumulation of minor setbacks conspired to delay progress on several fronts. Although the goals of the project have clearly not been fully achieved at this point, considerable progress has been made, and there is every reason to believe that the program objectives will be met in the near future.

Although we knew that the growth of the $ZrO_2 \cdot Y_2O_3$-W (ZYW) composite was far from an exact science, we felt that we could build on prior work in this area and make rapid progress toward solving some of the problems that had been plaguing the process over the years. However, a few of these problems, particularly that of "banding" in the structure (discontinuities in the growth of the tungsten fibers) proved to be more recalcitrant than expected. Nevertheless, an adequate amount of material with continuous fiber growth has now been made to fabricate a sufficient supply of samples to complete the proposed work. The composite growth work is discussed in more detail in Section A.1.

Etching of the composites also proved more difficult than anticipated. Previous work in this area suggested that there might be some problems in obtaining reproducible, etched structures with pointed pin tips, but we were unable to obtain any usable samples using the procedures detailed in previous reports. Fortunately, this led to an investigation of plasma etching, which may eventually provide better, and more uniform, pin tip geometries than were ever available with the chemical etches. The progress in this area is delineated in Section A.2.

In Section A.3, the work accomplished to date on LVFE structure development is recounted. This effort has suffered significant delays in the past six to nine months, when substantial activity was scheduled, from lack of adequate samples to work with, coupled with delays in bringing the e-beam evaporation facility on-line. However, these obstacles have now been overcome and work is expected to proceed rapidly in this area.

Most of the work on emission testing, addressed in Section A.4, has been associated with the set-up of a vacuum test station, design and assembly of a test vehicle, and collection of the associated electrical equipment needed for both the CW and RF electrical tests of the field emission cathodes. The test vehicle is suitable for tests up to 1 GHz, which should be more than adequate for this program.

One important aspect of this program was to investigate whether coatings or other emitter surface treatments would stabilize the work function of the emitter tips and thereby improve the uniformity of emission from the arrays. In order to evaluate the effect of these surface treatments, it is necessary to image the emission pattern from the arrays using a field emission microscope designed to project an image of the cathode surface. Considerable time and effort has been invested in the design and construction of this instrument, and we are still awaiting the delivery of several key components. When it is completed, however, it should prove to be extremely useful for characterizing the emission uniformity of field emitter array cathodes. The FEM is described in some detail in Section A.4, and we expect to report results of tests with this instrument in the final report.

II. TECHNICAL PROGRESS

A. Field Emitter Cathode Development

A.1. Composite Development

Directional Solidification

The directional solidification of eutectic systems can be accomplished in many ways. Central to all techniques is the need for a thermal gradient applied in a particular direction. This gradient provides the driving force for the solidification of the multi-phase system in one direction. For a binary eutectic system with the secondary phase present in quantities less than approximately 20 weight percent, directional solidification produces a fibrous secondary phase in a primary matrix.

For low temperature systems, conventional melting and thermal gradient techniques can be employed. For high temperature systems, less conventional techniques must be used to prevent contamination from the melt crucible, among other things. Such techniques include internal zone melting and skull melting.

Internal zone melting was the first crucible-less melting technique pioneered for high temperature systems. This technique couples an RF field at a frequency of 3 to 5 megahertz to a conductive material. In oxide systems, the conductivity at room temperature is normally too low to allow direct coupling. This problem can be alleviated by preheating the sample to a temperature where the oxide becomes conductive, after which direct coupling is possible. Concurrent increases in temperature, electrical conductivity and resistance heating with power continued to until the interior of the sample melts at temperatures up to 3000° C. The high radiant heat losses from the surface of the sample, combined with the low thermal conductivity of the oxide maintains the outer sample surface temperature below the melting temperature. This outer surface serves as a crucible

to contain the molten material without introducing impurities. Directional solidification can be accomplished by lowering the sample through the RF field.

The requirement for low thermal conductivity necessary to maintain the skin of the sample limits the oxide systems that can be melted with this technique. This limitation, combined with the inability to control the diffusion of oxygen in the melt led to the development of skull melting.

The technique of skull melting has many similarities to the internal zone technique. The melting is accomplished with an RF field between 3 and 5 megahertz. The sample preheating is typically accomplished with a graphite susceptor technique, where graphite in the form of a disc is placed in the sample and located in the field of the RF coil. The entire sample is placed in a water-cooled, copper crucible (Figure A.1.1). This maintains the skin integrity of the sample regardless of the sample's thermal conductivity. The ability to control the diffusion of oxygen into the melt is also increased. The sample is exposed to a 15 kilowatt RF field to melt the interior of the sample. Upon melting, the crucible is lowered through the field, solidifying the melt from the bottom of the sample to the top to produce an ingot as illustrated in Figure A.1.2. As the solidification front moves through the ingot, the tungsten precipitates as parallel, single-crystal fibers, 300-400 nm in diameter, spaced 3-5 μm apart. An example of the microstructure typically observed in such ingots is shown in Figure A.1.3.

The skull melting of yttria-stabilized zirconia/tungsten (ZYW) composites for use in Low Voltage Field Emitters evolved over a number of years to a point that the material was reasonably producible. The process and the samples produced were not defect free, however, with the principal defect being numerous discontinuities in the tungsten fibers (Figure A.1.4). These discontinuities in the fibers cause numerous problems in subsequent

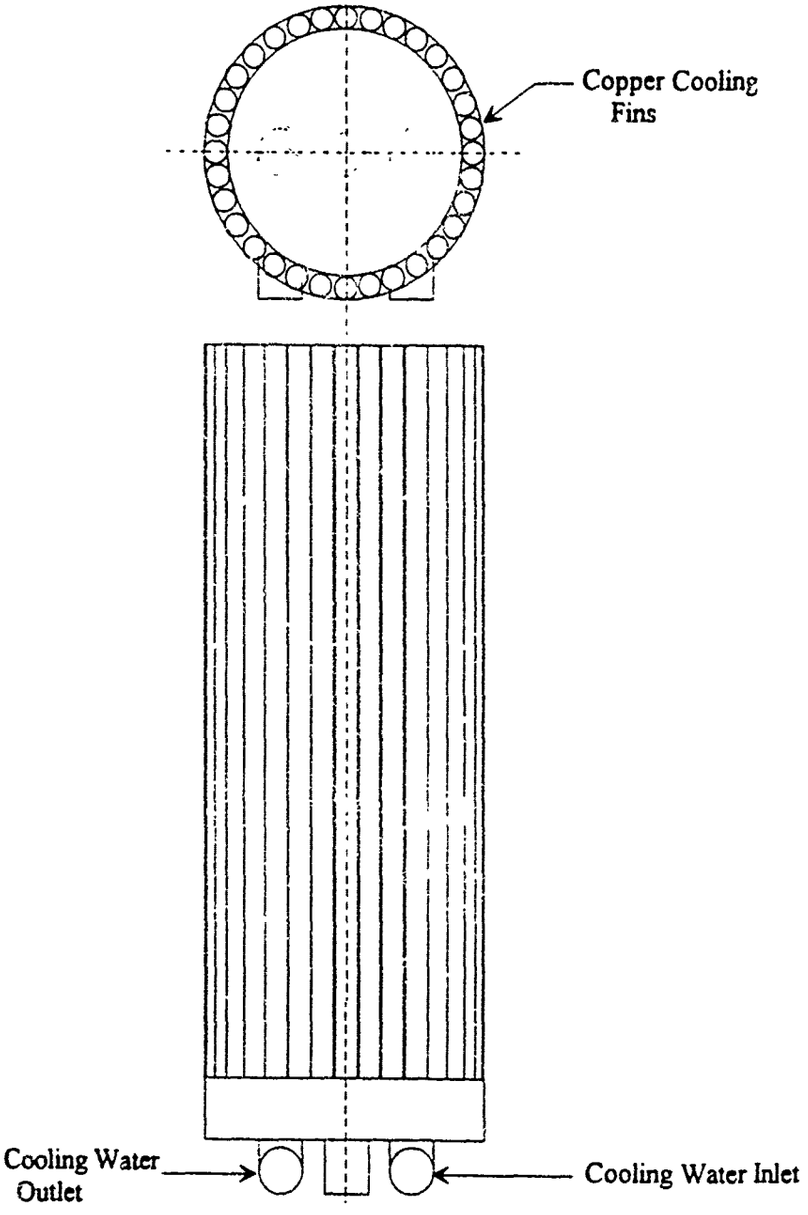

Figure A.1.1. Schematic of the Water-Cooled Copper Skull Used to Directionally Solidify the $ZrO_2 \cdot Y_2O_3$-W Composite.

Figure A.1.2. Photographs of (a) a Directionally Solidified Ingot and (b) a Sectioned Ingot.

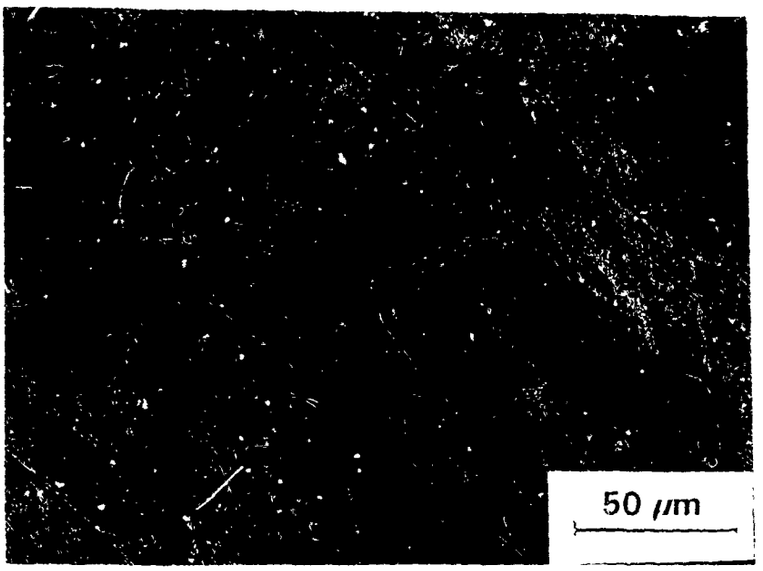

Figure A.1.3. Optical, Dark-Field Micrograph Illustrating the Typical Growth Morphology of the ZYW Composite.

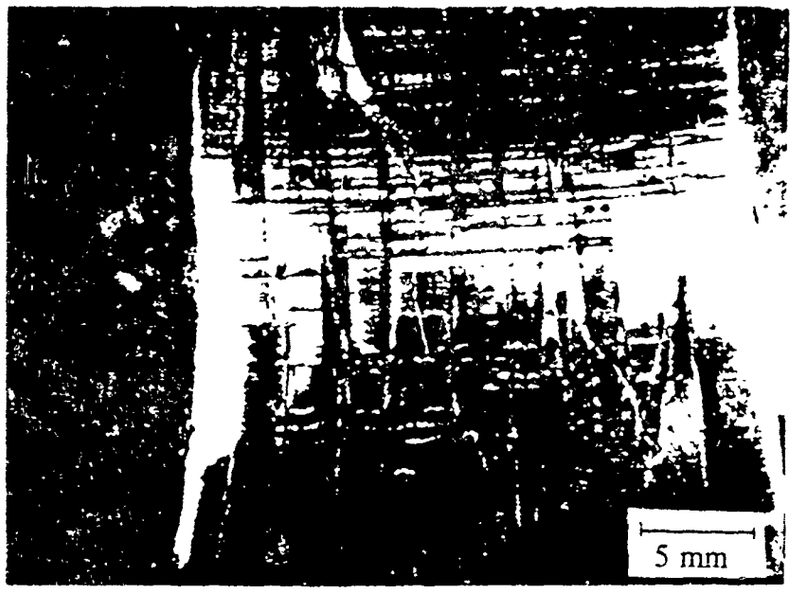

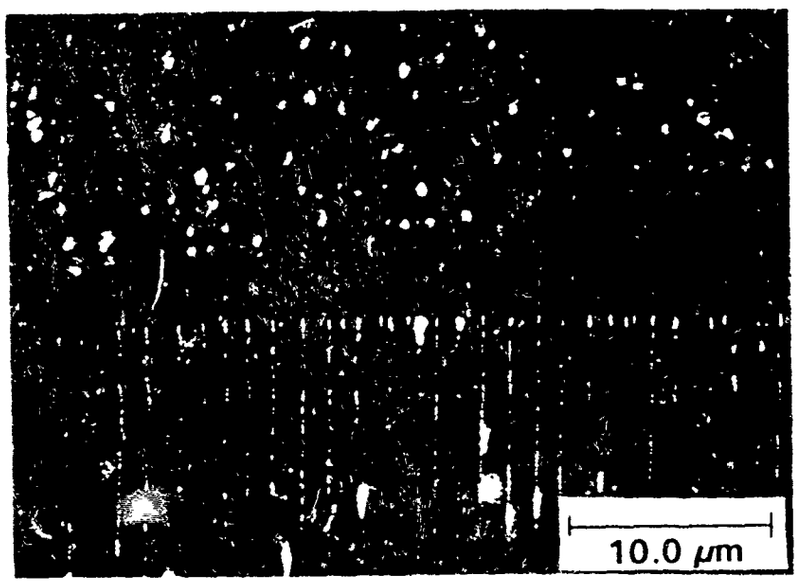

Figure A.1.4. Photomicrographs Illustrating the Principle Growth Defect in the ZYW Composite, (a) "Macroscopic Banding", and (b) "Microscopic Banding".

processing steps and often render a sample unusable. For example, when etching a banded sample to expose the tungsten fibers it is highly possible that the etching process will terminate in the banded region. This leaves the surface as it was initially; with no exposed fibers. Any bands in the interior of the chip also become a problem in the performance of the field emitters because the banded region provides unrecognized resistance in an otherwise continuous fiber.

To address the problem of fiber discontinuity, several steps have been taken to improve the process and thereby reduce or eliminate the banding in the composite samples. These steps include changes in the lowering control during composite growth, changes in powder handling practices, improved control of oxygen stoichiometry in the melt, and changes in the RF frequency used for heating.

Solidification Rate Control

Variations in solidification rate due primarily to uneven movement of the platform supporting the skull, both short and long-term, can lead to defects in the growth of the ZYW composite, which can, in turn, cause problems in subsequent processing steps of the LVFE cathodes. Low frequency ($< 10^{-3}$ Hz) variations in the solidification rate can cause variations in fiber diameter throughout the solidified composite.

The apparatus used initially to lower the skull employed a dc, variable speed motor, a gear reducer and a right-angle screw jack driving the platform on which the skull was mounted. The rotational speed of the motor, monitored with a strobe, was correlated to the lowering rate. Numerous runs were made with this system configuration until it was recognized that stray RF from the generator was interfering with the motor, causing gradual speed variations. The motor and its power lines were shielded, which reduced the motor speed fluctuations, but unacceptable higher frequency variations in lowering rate

persisted. The gears and screw jack in the motor-driven system introduced numerous points for mechanical friction and momentary sticking, and it was these factors to which the high frequency lowering rate changes were attributed.

An hydraulic lowering system was designed to replace the motor driven system, eliminating the effects of stray RF on the lowering rate, and the system was configured to eliminate as many potential mechanical friction points as possible. The system pressure was supplied by a manually-operated hydraulic pump. The hydraulic ram was extended to begin the run, and the weight of the skull, foundation plate and several hundred additional pounds forced the cylinder closed to lower the skull. The hydraulic fluid was routed through a precision needle valve as the platform was lowered, providing precise control over the lowering rate (Figure A.1.5).

A high-precision linear variable differential transformer (LVDT) was adopted to monitor the lowering rate, and allowed clear assessment of the magnitude of variations in the lowering rate. Figure A.1.6 illustrates the improvement in control which resulted from the adoption of the hydraulic system as opposed to the motor driven system. This improved control over the solidification rate reduced the occurrence of "macroscopic" banding, although closely spaced "micro" bands were still evident. In an effort to eliminate these bands, additional variables were addressed.

Materials Handling

Historically, the material processing steps included hot pressing the zirconia (yttria-stabilized)-tungsten powder mixture to between 85 and 90 percent of the theoretical density, crushing this material to 10 mesh, and mixing the crushed material with additional yttria-stabilized zirconia powder to yield a pressable material of appropriate overall composition. This mixture was then dry pressed to an average of 55 percent of theoretical

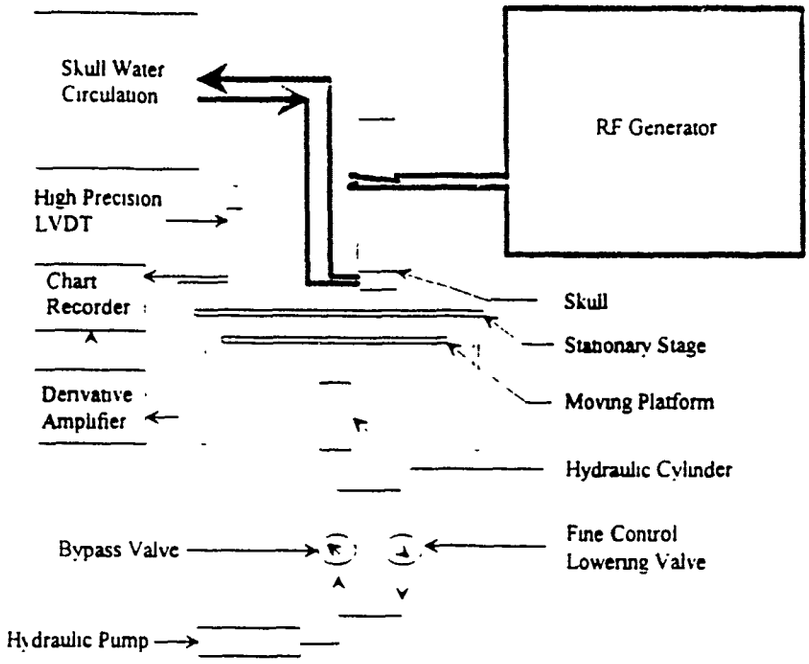

Figure A.1.5 Schematic Diagram of the Hydraulic System Used to Control the Lowering Rate of the Skull Platform.

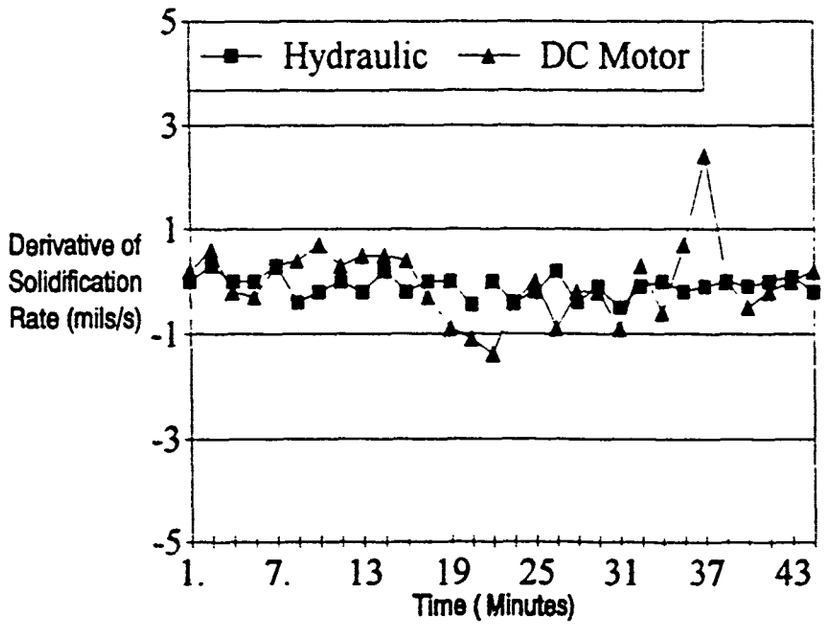

Figure A.1.6 Comparison of the Effect on the Lowering Rate of the Skull Platform using the Hydraulic System and the DC Motor/Reduction Gear System.

density, and these low-density pellets were loaded into the skull (Figure A.1.7) and melted. The density of the pellets represented a compromise between material supply for the melt and power required for melting. A higher initial density would require more power for melting than the 15 KW generator could supply, while a lower density would not supply sufficient material to the melt to sustain solidification over an appreciable time, resulting in very small ingots. The ingots obtained from this process, with few exceptions, yielded significant quantities of usable, albeit banded, material along the entire length of the ingot. This baseline procedure was, however, extremely time consuming and iron impurities were introduced during the crushing of the hot pressed material; in an effort to alleviate these shortcomings alternative procedures have been investigated.

The first alternative studied was to simply use the yttria-stabilized zirconia and tungsten powders as they were received from the vendors. The powders were mixed, using the same composition as the pellets, loaded into the skull and melted. This technique produced ingots with a limited region of fiber growth occurring at the bottom of the molten zone (that is, early in the solidification process), and the regions in the ingot containing satisfactory growth were smaller than those obtained using the baseline process. The area immediately above the region of good fiber growth contained large areas of primary oxide, with tungsten fibers growing around the periphery. The top portion of such ingots contained a considerable amount of a greenish material, indicating the presence of a mixture of tungsten oxides. These three regions extending from the bottom to the top of the ingots, indicated that the melt initially contained sufficient tungsten in solution for growth, but the tungsten content was apparently decreasing as solidification continued, causing fiber growth to degenerate. Since the tungsten oxides are quite volatile, it is likely that a portion of the tungsten is oxidizing and vaporizing before it goes into

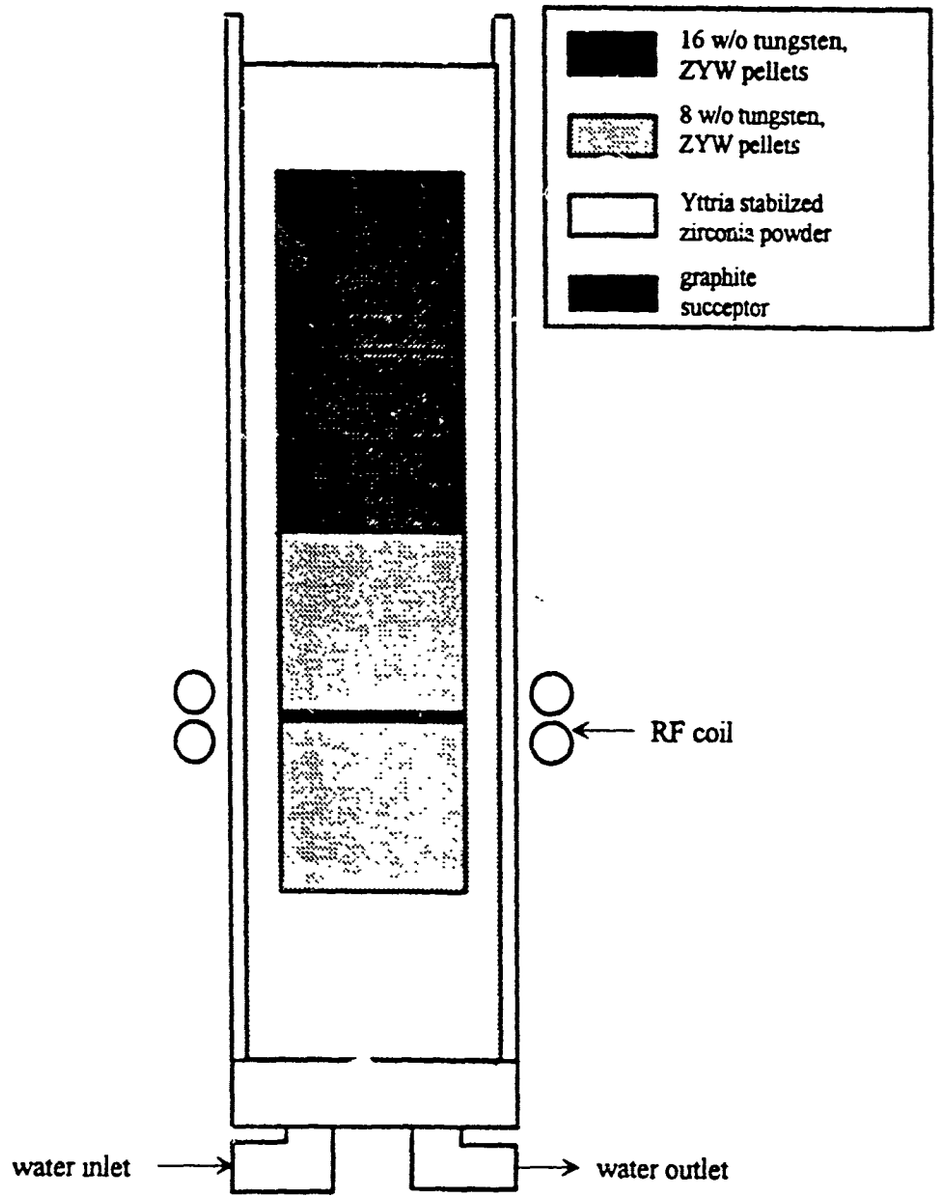

Figure A.1.7 Schematic of the Initial Configuration of the Skull, Showing the Position of the Hot-Pressed Pellets and Graphite Susceptor.

solution. These growth results were also noted to be less reproducible than results from the baseline process.

It has been noted that zirconia reduces at temperatures above 1000° C. Clearly, the oxygen given off, if evolved in sufficient quantities, could oxidize the tungsten to a state that would sublime at temperatures below the melt temperature. The resultant loss of tungsten would reduce the supply available for fiber growth, resulting in smaller regions of growth and larger regions of primary oxide. Previous experiments in this system have suggested that the tungsten must, however, be oxidized to a limited degree before sufficient quantities will go into solution in the molten zirconia. At the solidification front, the (reduced) zirconia apparently takes up any excess oxygen, allowing tungsten metal to precipitate as fibers. Considering this apparent sensitivity of the system to oxygen content, a dedicated effort is planned to study the effect of residual oxygen in the zirconia powder on composite growth.

Another procedure evaluated involved the pressureless sintering of dry pressed yttria-stabilized zirconia-tungsten pellets in a controlled atmosphere in an effort to reduce the zirconia and remove the liberated oxygen before the melting process. Additionally, the sintering operation was intended to yield pellets with the proper density so that further processing steps would be unnecessary. The sintering operation was performed in argon-4% hydrogen at one atmosphere in an Astro, tungsten element furnace. The firing schedule was comprised of a temperature ramp at 10° C/min with a one hour hold at 1600° C, followed by a 25° C/min cooling rate. Although the pellets obtained were reduced on and near the surface, they displayed evidence of tungsten oxidation in the interior. A higher sintering temperature of 1800° C on a similar schedule was tried, yielding comparable results. The last sintering procedure tried in the $Ar/4H_2$ atmosphere

used a temperature ramp at 2° C/min to 200 degrees, followed by a one hour hold, which was incorporated in an effort to eliminate adsorbed water and oxygen from the pellet at the lowest possible temperature. The temperature was then ramped at 8° C/min to the final temperature of 1800° C. The results from this sintering procedure indicated more extensive zirconia reduction, but there was still a considerable degree of tungsten oxidation observed in the pellets. The oxidation that persisted was attributed to the fact that the relatively low percentage of hydrogen did not provide sufficiently strong reducing conditions to remove oxygen liberated from the interior of the pellets. All sintering procedures produced pellets of appropriate density.

All ingots solidified from the sintered materials described had small regions of growth at the bottom of the ingot, but displayed a large area of the primary oxide structure that was first evident in the ingots derived from dry pressed powders. This was attributed to tungsten oxide that was formed in the sintering steps and which, when heated by the molten zone, was volatilized, thus depleting the melt of tungsten at the top.

In an effort to capitalize on the information from the described experiments, one additional procedure was evaluated. This process was envisioned to obtain comparable results to those of the baseline process while avoiding the introduction of iron impurities and without the large investments of time. The ability to reduce the zirconia without oxidizing the tungsten while tailoring the density of the pellets were specific objectives. In this process, the zirconia and tungsten powders were mixed and dry pressed only to pressures that allowed handling while not accomplishing any appreciable compaction. These green pellets were loaded into a graphite die, intended to provide a strongly reducing atmosphere at high temperature, and heated to approximately 1600° C. Once this temperature was reached, pressure was applied to compact the pellets to the desired

densities.

The skull-melted ingot obtained from the graphite die sintering contained a much larger region of growth than any of the previous experimental approaches. There was an area of primary oxide in the ingot, but it was smaller than before. The presence of this region implies that some of the tungsten supply was lost to oxidation. The green oxide, characteristic of tungsten oxides, was present in this ingot but to a lesser extent than in ingots of the previous alternative processes. The growth in the ingot contained some micro-banding and several small bands that spanned the entire cross-section of the ingot. Macroscopic bands were not present.

Through the use of high temperature thermogravimetric analysis and x-ray diffraction, planned efforts will attempt to correlate the extent of zirconia reduction with growth characteristics. Once this investigation has been completed, a substantially improved composite growth procedure will have been established.

Frequency Variations

Several investigators have reported banding in solidified RF melted Al-Cu alloys. Elimination of the banding in the solidified material was accomplished by changing the RF frequency. Although this phenomenon was observed in a metal system, it is believed that frequency may have a similar effect on the continuity of the tungsten fibers in this system.

In the present equipment, an RF frequency between 4 and 4.1 Mhz is used. Using another available generator in which the frequency can be varied from 2.5 to 4 MHz, the effect of frequency on the continuity of the tungsten fibers will be examined.

A.2. Emitter Tip Geometry and Composition

One of the most critical steps in the formation of the arrays of emitters which comprise the LVFE cathode is the process of etching the ZYW composite to expose the tungsten fibers to a specific length and form the sharply pointed conical tips.

The $ZrO_2 \cdot Y_2O_3$ matrix of the composite is extremely inert to most etchants, and it is necessary to use hot phosphoric acid to dissolve the matrix of the composite. The chemical etching apparatus is shown in Figure A.2.1. It consists of a PYREX flask containing the etching solution attached to a reflux condenser. The ZYW samples are suspended in the solution using glass supports. The reflux condenser is used to maintain the concentration of the acid solution at a constant value, since the etch rate is dependent on both the temperature and concentration of the etch bath. The temperature of the bath is maintained using a heating mantle controlled with a proportional temperature controller, with the temperature sensed by a type J thermocouple.

The H_3PO_4 acid is normally supplied at a concentration of 85%. It is further concentrated by heating at a specific temperature, with the condenser off, until it boils. At that point, the condenser is turned on, maintaining the concentration at a constant value. Since the relation between the boiling point and concentration is known, this process allows the concentration of the solution to be selected with considerable precision.

The tungsten fibers are not affected by the pure H_3PO_4 solution; thus it can be used to expose the fibers to a specific length. The rate of dissolution of the $ZrO_2 \cdot Y_2O_3$ matrix is strongly temperature dependent, and highly reproducible at a given temperature. The temperature also has a marked effect on the surface topography, an effect first described

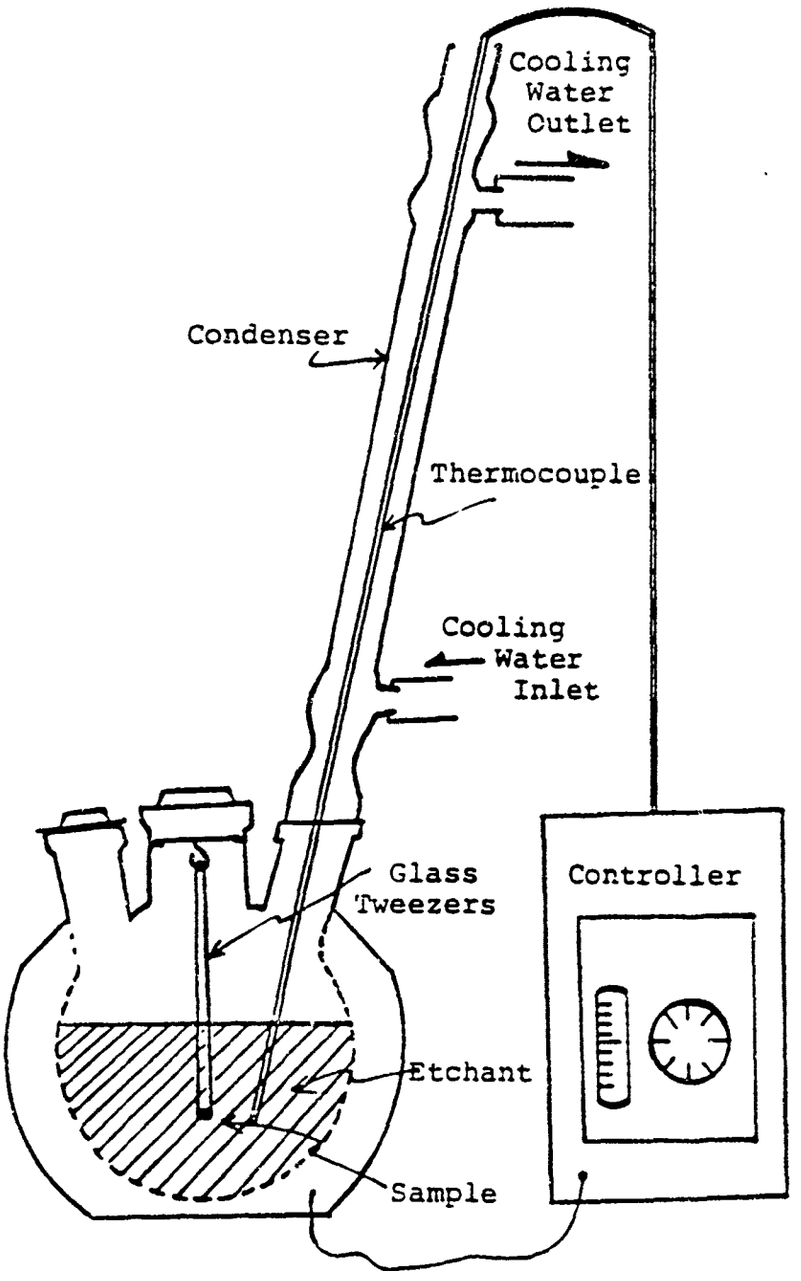

Figure A.2.1. Schematic of the Apparatus Used to Chemically Etch the ZYW Composite Chips.

by Moh[1] and corroborated in this study. At temperatures above 210° C, it was noted that hillocks formed around many of the tungsten fibers, while at temperatures below 210° C, etch pits were observed around the fibers. Since a relatively smooth matrix could be maintained at the 210° C temperature , all of the etching was performed at this temperature. The data shown in Table A.2.1 illustrates the relationship between etching time and fiber height using the pure H_3PO_4 etch.

Table A.2.1: Pin Heights of 95 % H_3PO_4 at 210 °C.

Time (hrs.)	Pin Height (μm)
1.1	1.5
1.5	2.0
1.75	2.5
2.0	3.0
2.25	3.5

Hillock formation around each fiber, as a result of the etch temperature being too high, is illustrated in Figure A.2.2. This micrograph also illustrates the effect of irregular fiber growth on the shape and size of the etched fibers. In the sample shown in Figure A.2.3, pits have formed around many of the fibers. Unfortunately, hillock and pit formation have also been observed on the same sample, suggesting that their formation is also dependent on the crystallographic orientation of the grains. The variation of fiber length with etching time was confirmed to be linear in the range of fiber lengths produced

[1] K. H. Moh, M.S. Thesis, Georgia Institute of Technology (1983).

Figure A 2.2 Illustration of Hillock Formation Around Fibers After Etching with 95% H_3PO_4 at 240 °C for 70 Minutes. Pin Height is 1.2 μm

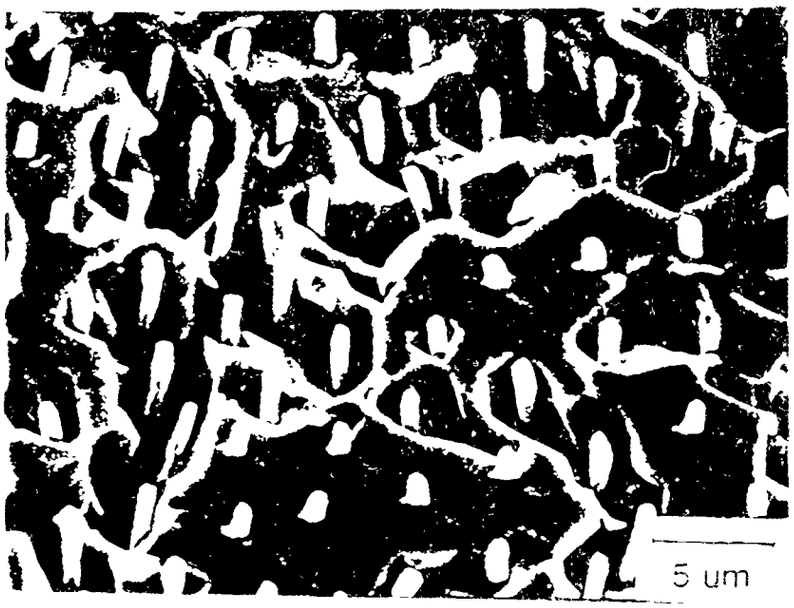

Figure A 2.3 Illustration of Hillock Formation Around Fibers After Etching with 95% H_3PO_4 at 240 °C for 70 Minutes

thus far (1.4 μm to 3.5 μm).

The ZYW composite ingot contains many low-angle grain (cell) boundaries, and most samples had some "cells" in which etch pits were formed around the tungsten fibers despite the fact that the etch temperature was correct. These etch pits are related to the crystallographic orientation of the grains and are more pronounced in some grains than others. They are thought to be due to stresses introduced either in the solidification process or during the grinding and polishing operation. This defect was substantially reduced by annealing the ground and polished samples, prior to etching, for 1 hour at 1,500° C in a reducing atmosphere (Ar, 4% H_2). Although etch pits still appear in a few grains, their size is much smaller and, in most of the grains, the matrix shows no tendency toward pitting. This is illustrated in Figure A.2.4, which shows two samples with different pin heights.

Pointed Pin Etching

Once the pure H_3PO_4 etch process was under control, several attempts were made to produce pins with sharply-pointed conical tips. This requires a mixture of hydrofluoric (HF), nitric (HNO_3), and H_3PO_4 acids, heated to ~200° C. The combination of HF and HNO_3 dissolve the tungsten, and by regulating the amount of each of those acids in relation to the H_3PO_4, it should be possible to etch the tungsten fibers at a slower rate than that of the ZrO_2 matrix, giving sharply pointed conical pins.

Several concentrations were investigated, first keeping both the HF and H_3PO_4 concentration fixed and varying the quantity of HNO_3; and later varying the HF concentration relative to that of the H_3PO_4 and HNO_3 acids. The results are presented in Table A.2.2. There was considerable variation in both the pin length and tip geometry. In almost every case, attempts to obtain shorter pin heights resulted in complete removal of

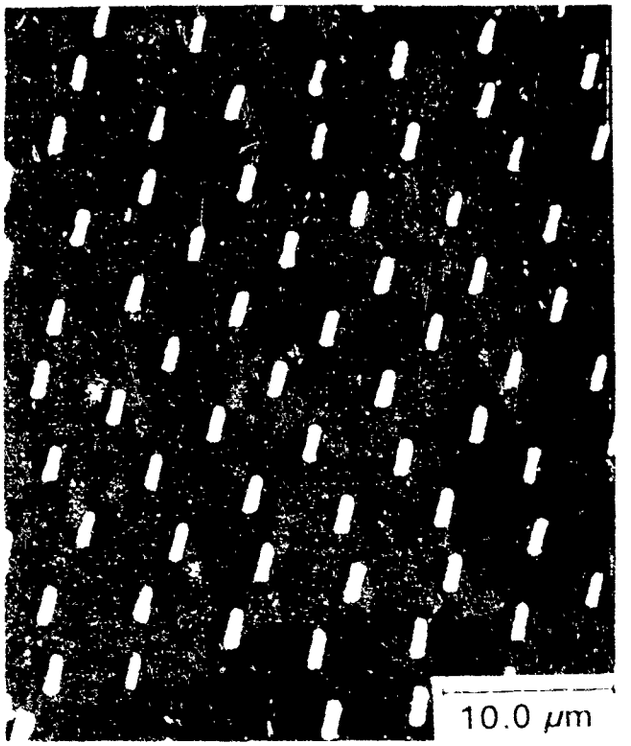
10.0 μm

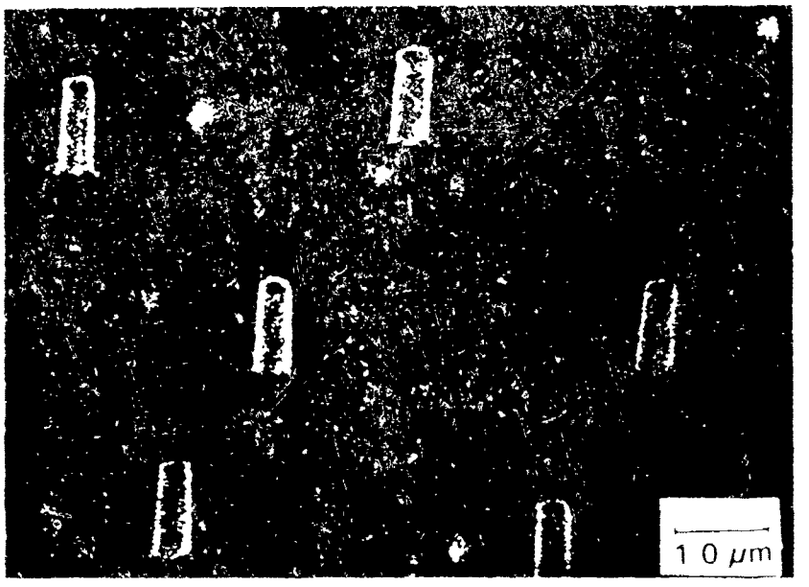
1 0 μm

the fibers. All the data in Table A.2.2 was obtained at a specific time period (105 minutes), but a one-hour etch time was also used for both Etch 1 and the Etch 4 to see if the tungsten dissolution rate could be reduced. In the case of Etch 1, the same pin height

Table A.2.2: Pin Heights and Acid Concentrations for Pointed Pin Etching.

Etch No	Vol. of HF (ml)	Vol. of HNO_3 (ml)	Vol. of H_3PO_4 (ml)	Pin Length (μm)
1	2.5	2.5	100	5
2	2.4	2.5	100	0
3	1.25	2.5	100	0
4	1.0	2.5	100	0
5	2.5	2.0	100	0
6	1.0	2.0	100	6

was obtained but with larger tip radii, whereas Etch 4 still dissolved the fibers.

Figure A.2.5 shows pointed pins obtained with Etch 6 at 210 °C for 1.75 hrs. A Pin height of 7 μm was obtained for this specific sample but other tests gave 6 μm pins. In Figure A.2.6 one can clearly see the etch pits formed when the etch composition was modified to try and increase the pin cone angle and thereby reduce the pin height.

One possible explanation for the variable etch rates obtained with the fiber pointing etches is the high volatility of hydrofluoric acid, which makes it extremely difficult to maintain a constant acid concentration, even with the reflux system on. In addition, the more aggressive nature of the etch makes the process much more sensitive to matrix roughness.

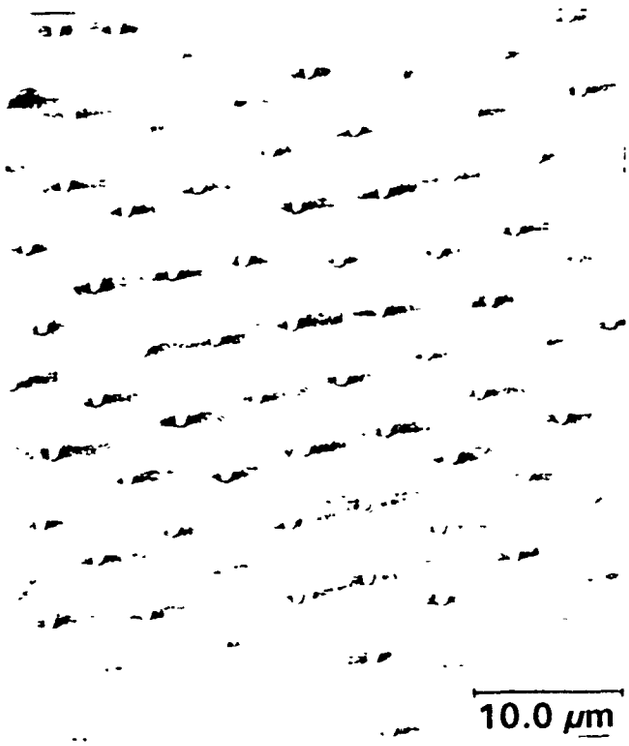

Figure A.2.5. Sharply Pointed Exposed Fibers Obtained with the Fiber Pointing Etch No. 4; Pin Height: 7 μm.

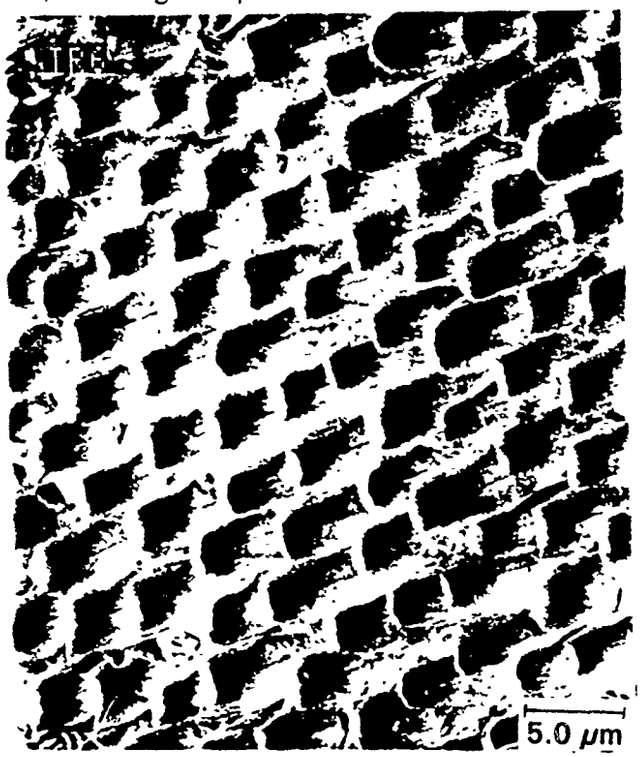

Figure A.2.6. Pitted Surface of the Composite Resulting from a Test of Fiber Pointing Etch No. 3.

There are so many variables involved in the etching process (time, temperature, and numerous composition variables) that the experimental matrix quickly becomes quite large. Add to this the time-consuming nature of the tests (the result of each experiment must be evaluated in the SEM), and it is not surprising that progress in this area has been slow. However, work is continuing in this vital area, and the more recent results have been encouraging.

Plasma Etch Processing for Fiber Pointing

As an outgrowth of efforts to develop photolithography techniques for the purpose of defining emitter areas of precise size and shape (described in a subsequent section), it was recognized that plasma etching showed promise as a method for producing conically pointed emitter pin geometries. The chemical procedures had proven quite satisfactory in earlier work using UO_2-W composites, but the $ZrO_2 \cdot Y_2O_3$-W materials, which are being pursued exclusively in this work, are substantially more difficult to etch chemically. When it appeared that the plasma etching being utilized in development of the photolithography techniques for cathode patterning held promise as a means of emitter tip pointing, it was decided to pursue the process in parallel with, and as a possible alternative to, the chemical etching method.

Initial results indicated that plasma etching held the potential for producing sharply pointed emitter tips, equivalent to those produced by chemical etching, but without the problems of matrix surface roughness described above. The initial, serendipitous observation of the ability to point the tungsten emitter pins is shown in the scanning electron micrographs of Figure A.2.7. The irregularity of the zirconia matrix surface noted here is a product of the initial chemical etching used to expose blunt, unpointed tips and is not

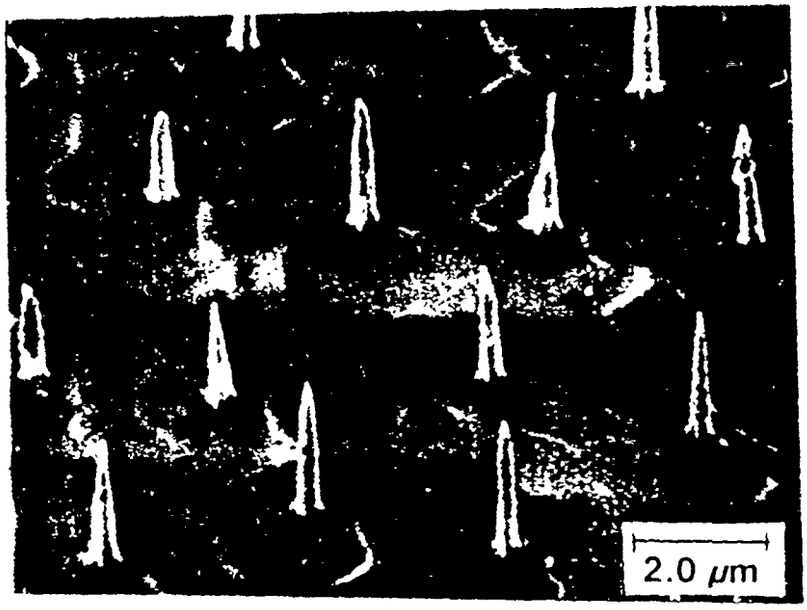

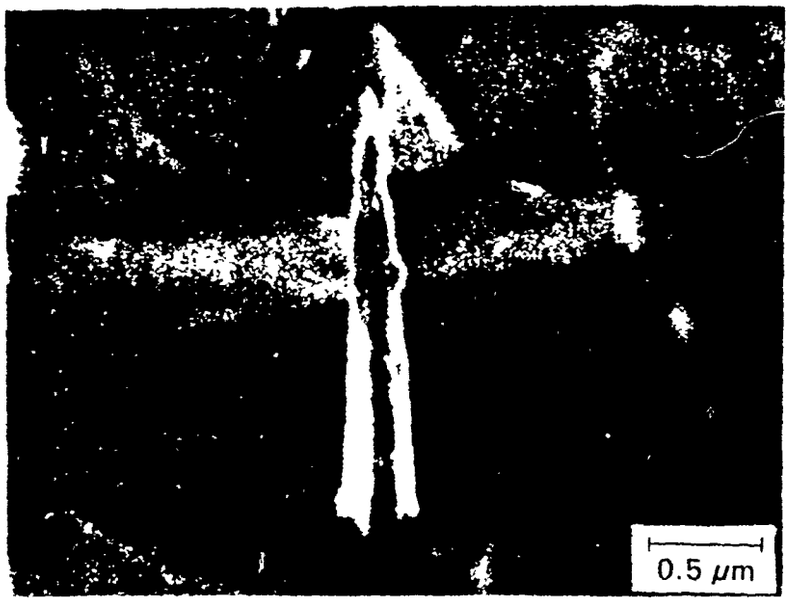

Figure A 2 7 Scanning Electron Micrographs Showing Initial Observation of Tip Pointing Obtained by Plasma Etching.

a product of the plasma etching process. The matrix condition routinely observed subsequent to exposure of the composite to the fiber pointing etches is notably worse than the minor surface roughness observed here. Furthermore, it was thought likely that the plasma etching procedure would have distinct advantages in providing a reproducible process.

Plasma Etch Procedure

The process of obtaining pointed emitter tips using plasma etching is conceptually quite simple. A composite sample is first polished and then selectively etched using the processes described earlier with the use of hot phosphoric acid to expose the tungsten fibers to a few micrometers in height. This process can generally be considered reproducible, and a smooth matrix surface is typically obtained. The latter issue requires further evaluation and development, but the ability to produce blunt fibers with a smooth matrix is undoubtedly better than the chances of chemically etching pointed tips with comparable matrix quality. Typical sample condition at this stage is similar to that shown in Figure A.2.4.

Next a photoresist layer is spun on, its thickness being just sufficient to cover the exposed fibers. After baking (and patterning by exposure and development as appropriate, as described in Section A.3.) the resist covered sample is subjected to the plasma etch. The critical factor in the etching, analogous to the chemical etching process for fiber pointing, is simultaneous etching of the resist (analogous to the matrix in the chemical process) and the tungsten fiber, with the resist etching rate being greater than that for the tungsten. If the two etch rates are suitably balanced, the etching of the resist proceeds to continuously expose unetched portions of the fiber allowing etching to start. However, any portion of the fiber above a given point will have been exposed to the plasma for a longer

period, and will have experienced material removal for a longer period. This dynamic process naturally leads to the formation of a conical point, and can be stopped at any desired point, up to the time at which all resist is removed, to provide pointed emitter tips.

If etching is stopped before complete removal of the resist, a pin geometry consisting of a conical tip on a straight, cylindrical shank results. If etching is continued beyond the time when resist removal is complete, then obviously removal of material from the pin continues, relatively uniformly (neglecting any anisotropy in the etching, which does appear to be an issue as yet unexplored), and will first result in blunting and finally recession of the pin into the matrix as described in Section A.3. which reports work on the photolithographic patterning of emitting areas.

Initial work based on the early observation of pointed tips used the planar etching system which had been being used for work on the lithographic process. This system produced very encouraging results as shown in Figure A.2.8., which provides an example of emitter tips at an intermediate stage in the plasma etching. Here the photoresist has not yet been completely removed, the material between pins is photoresist, but the pins have clearly been sharpened by the plasma etch. These results were obtained using a commercial gas mixture, PDE-100, which consists of carbon tetrafluoride and oxygen, etching for a period of thirty minutes.

Continuing work in this system encountered serious sample contamination problems consisting of aluminum and fluorine, as identified by energy-dispersive x-ray analysis in the scanning electron microscope. This contamination seemed initially to appear randomly, and some significant period elapsed before investigation showed that it was a product of the etcher itself. The vessel in which the etching process was performed is aluminum,

which unless coated with a layer of vapor deposited silica, will react with the etch gas to form aluminum fluoride, which in turn will deposit on the sample during processing. The aluminum fluoride deposited on the tungsten pins allows continuing etching of the tungsten to take place, resulting in hollow aluminum fluoride shells which replicate the tungsten fibers. For some time the fluoride shells were believed to be the tungsten fibers, but puzzling disappearance of the fibers in subsequent processing led to identification of the contamination problem. The problems in the planar system were resolved by recoating the interior walls of the chamber, but this time consuming process (two to four hours) must be repeated after about thirty to sixty minutes of etching. As an alternative it was decided to try a barrel etcher which used a glass vessel with minimal metal in its interior.

This equipment proved to immediately resolve the contamination issue, and as an additional benefit appeared to significantly reduce the required process time. An extensive series of experiments has been performed in the barrel etcher which have resulted in significant progress, but which leave several unresolved issues at this writing.

Although a reasonably standard procedure was established early in the experiments, using a consistent pumpout procedure, controlled pressure of during etching, and a standard power level of 350 watts, it was noted that reproducible etch rates of the photo-resist were not obtained. Ultimately, some of the details of the process have been revealed, and it is now appreciated that under the normal etch conditions the rate of removal of the resist is initially quite high, of the order of 0.2 micrometers per minute. This should lead to complete removal of resist layers of the order of 1.5 to 3.0 micrometers thick in less than fifteen minutes. However, the results indicate that the rate of etching appears to decrease rapidly as a function of etching time. Analysis of resists once etching has dramatically slowed has clearly shown the presence of fluorine, and discussion with

the resist manufacturer has revealed that a process of "teflonization" is likely to occur under the etch conditions if etch times are overlong.

In addition, an effect of sample surface area has been noted. In order to facilitate handling of small composite chips, often a few millimeters in dimension, it has been common practice to mount the chips on two inch diameter silicon wafers using photoresist during the resist application, exposure and development. Generally the plasma etching has also been performed with the chip mounted on the wafer. In investigating whether or not thermal effects (temperature rise due to ion bombardment) were a factor in the etch rate problem it has been found that chips of up to about a centimeter in dimension not mounted on wafers appear to etch rapidly; however, if similar size or smaller chips are etched mounted on wafers, there is a rapid decrease in etching rate over a period of a few minutes. This effect is the subject of continuing investigation.

Results to date are extremely promising. A recent sample is shown in Figure A.2.9. The matrix surface morphology is that produced by the initial chemical etching, and while the overall pin height is greater than desired for current array fabrication practice, it is a straightforward issue to start the process with fibers of 1-1.5 micrometers in height rather than the fibers of approximately 3.5 to 4.0 micrometers height which served as the starting point for the sample in Figure A.2.9.

Conclusions

While there is still significant process development work to be done, and more detailed understanding of the plasma etching process by which emitter tips can be pointed is a necessity, it is clearly evident that a unique new process has been identified and basic understanding of many of its salient features obtained.

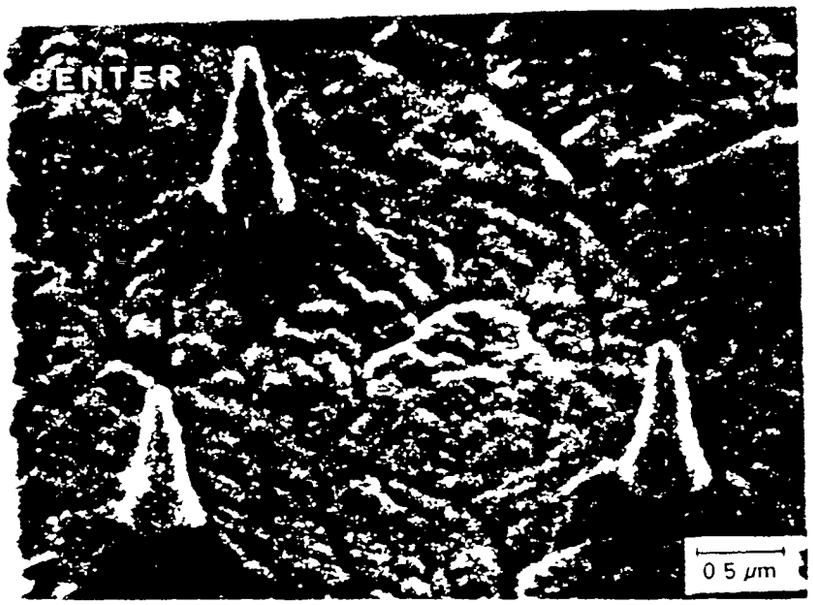

Figure A 2 8 Plasma Etched Sample before Completion of Process, with Pin Tips Protruding above Photoresist Layer

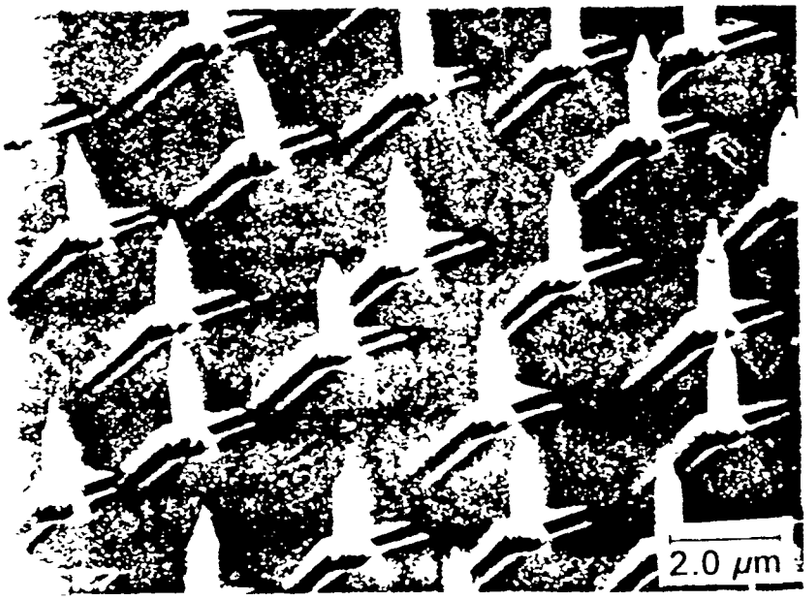

Figure A 2 9 Pointed-Pin Array after Completion of the Plasma Etching Process. (The matrix morphology was a result of the initial chemical etch used to expose the fibers.)

The advantages of this process are several, but the most important is undoubtedly its ability to be used in line with the photolithographic process being developed for patterning of arrays allowing precise definition of emitting areas. Use of the plasma etching process to point the fibers in the emitting areas, while simultaneously using the same procedure to remove the tips from areas outside the desired emitting areas significantly simplifies emitter fabrication relative to any fabrication process flow previously envisioned or investigated. Continued development of this method is expected to pay substantial dividends in establishing a consistent, reproducible fabrication process.

A.3. Field Emitter Structure Development

Definition of Emitting Areas by Photolithography

In earlier work at Georgia Tech the need to precisely define emitting areas of a prescribed size and shape was not an issue, so a technique utilizing a wax droplet to protect fibers in a randomly sized and located area was sufficient. Subsequent to removal of the tungsten fibers from the unprotected area of the sample, a single emitting area (on each individual chip), approximately circular in shape, was obtained by selectively etching the matrix, using chemical means, to expose and shape the tungsten emitter tips.

Experience with the zirconia-tungsten composite material had shown that obtaining smooth matrix surfaces, when using etch compositions needed for pointing of the emitter tips, was problematical. A smooth matrix surface is a necessity to assure good insulating film and grid integrity in subsequent deposition operations.

A need for development of a lithography based procedure, allowing definition of multiple emitting areas of precisely defined size and location, was identified as a requirement in the program.

The initial approach was to investigate the substitution of patterned photoresist for the wax droplet of the previous fabrication process. If successful this would allow direct adaptation of the earlier procedure, substantially simplifying requirements for involved process development.

Extensive experimentation demonstrated that neither, available, positive nor negative resists would withstand the strong alkaline (sodium hydroxide/potassium ferricyanide) or acid (hydrofluoric/nitric) aqueous solutions needed to selectively remove the tungsten fibers from the composite in the areas unprotected by the patterned resist.

Several alternative approaches, including electrolytic etching in weak basic solutions, which was initially thought to have significant promise, all proved to be unacceptable. Only one approach, namely plasma etching of the tungsten using a carbon tetrafluoride/-oxygen mixture (commercially available, PDE-100) proved to show real promise.

Initial development of such a process began with direct substitution of the plasma etch for the chemical etch, with the resist in place, patterned to protect the fibers in the intended emitting areas. This approach proved to remove the tungsten from the matrix, but the removal depth was limited (although probably sufficient for the purpose) and etching of the resist by the plasma proved to require extremely complex processing to provide an aluminum layer on the resist as an etch stop. In the course of this work the serendipitous observation was made that the plasma etch was capable of pointing the tungsten emitter pins, in a fashion analogous to the historically used chemical procedure, as described in an earlier section of this report.

At that juncture, a substantially simpler process was envisioned, which has subsequently remained the focus of continuing process development efforts. That process, as envisioned, has in essence been demonstrated, and continues to undergo development and

further refinement.

To demonstrate the ability to successfully define emitting areas of precise configuration and to provide suitable emitters for testing and evaluation in the course of the program, a mask set was designed which would allow simultaneous processing of sixteen separately addressable emitting areas, each 0.1 cm^2 in area, on a composite chip of about 3 mm x 3 mm dimensions. It was considered likely that as composite growth was improved, resulting in larger chip areas becoming available (up to 1 cm x 1 cm was the objective), that nine of the 3 mm x 3 mm chips could be simultaneously processed, to be snapped apart at the end of fabrication.

The mask set consists of three layers. The first to define the emitting areas; the second to define the corresponding grids (with leads to the outside of the pattern to facilitate electrical connection); and the third to define deposition areas for gold on the connecting pads at the end of the leads where beam lead attachment is made to the molybdenum grid film. The three masks are shown in the micrographs of Figure A.3.1., and a test pattern from the masks, laid down on a silicon substrate for evaluation is shown in Figure A.3.2. Patterning of a resist, via exposure and development, using the grid mask is shown in Figure A.3.3., demonstrating the suitability of the mask set for the intended processing.

Application of the first mask to the zirconia-tungsten composite material, as envisioned for emitter fabrication, is demonstrated in Figure A.3.4. The series of micrographs show the exposed pins corresponding to what would become the sixteen, discretely addressable, emitting areas with the subsequent deposition of the insulating layer (covering the entire sample surface) and the grids (with their areas defined to correspond to each of the emitting areas by the second mask).

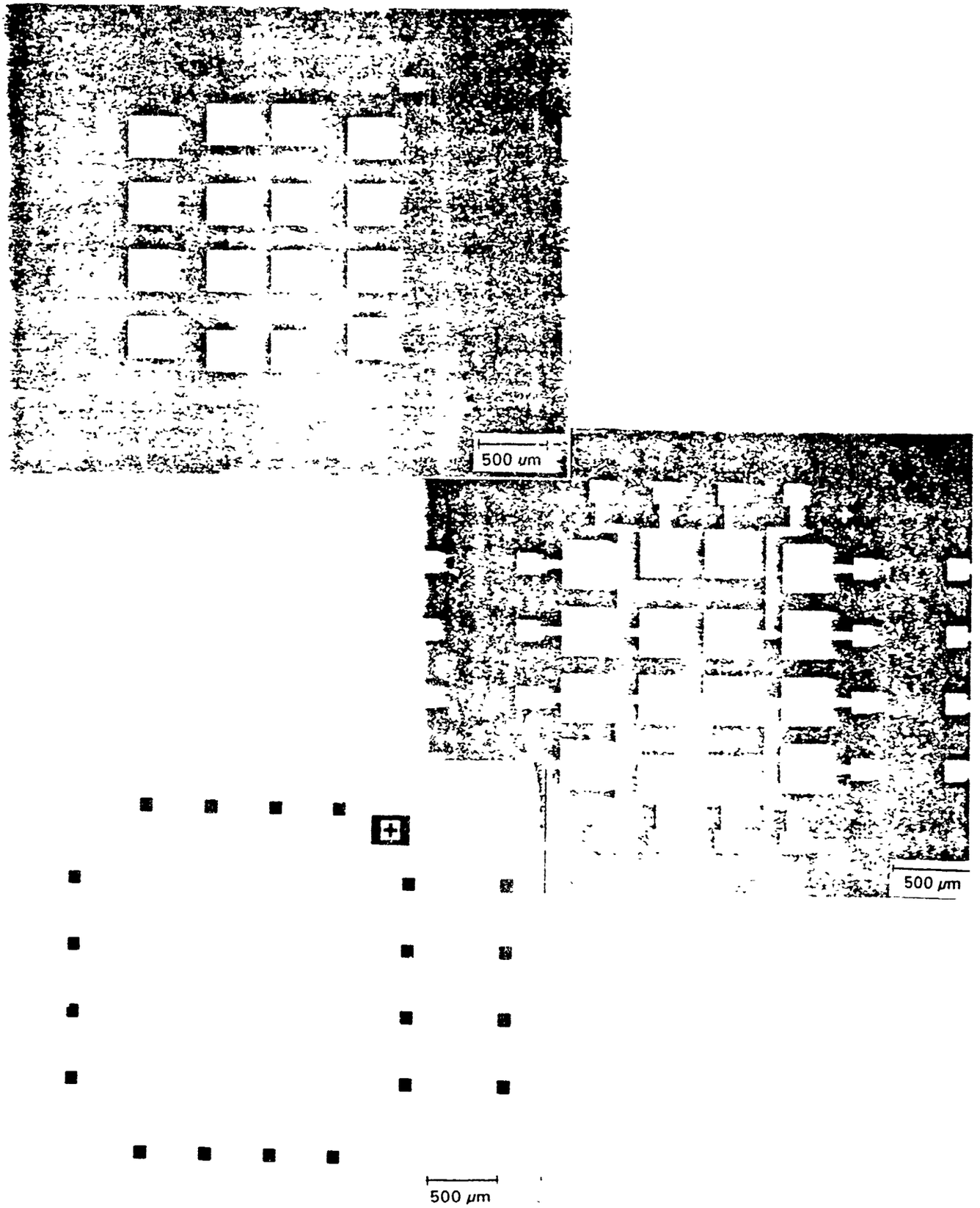

Figure A.3.1 Three Layer Mask Set for Georgia Tech Field Emitter Array Cathode Fabrication Process

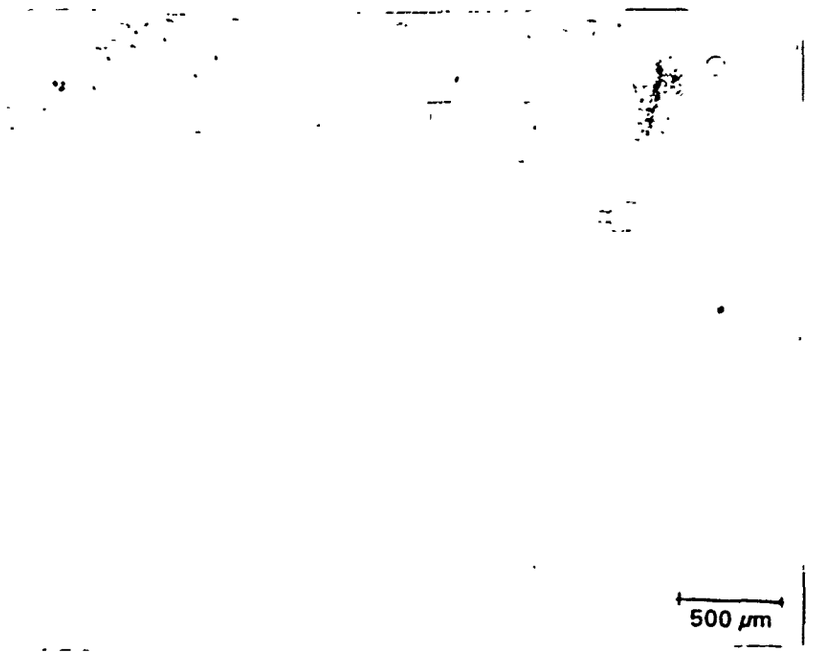

Figure A.3.2. Demonstration Pattern for the Mask Set on a Silicon Wafer.

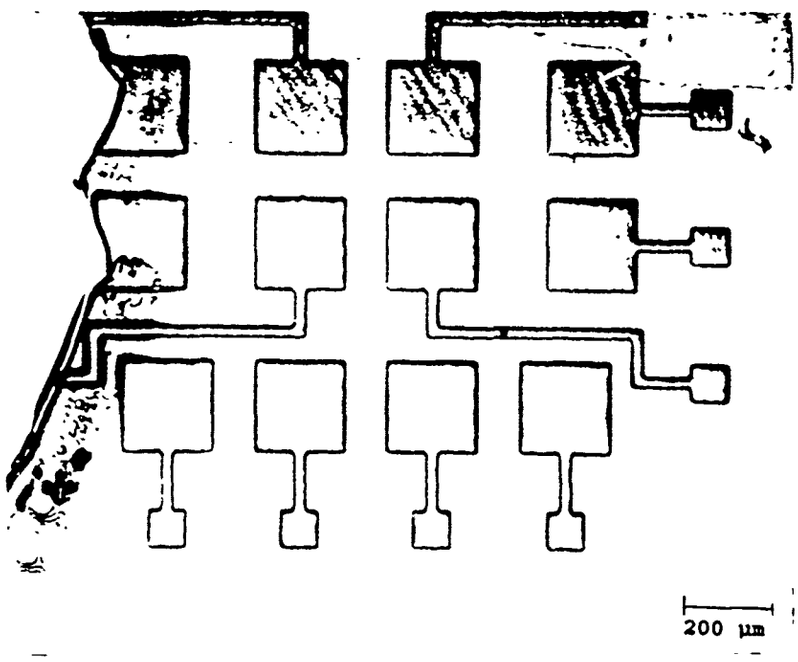

Figure A.3.3. Patterned Resist Showing the Pattern of Sixteen Grids and Their Connecting Leads.

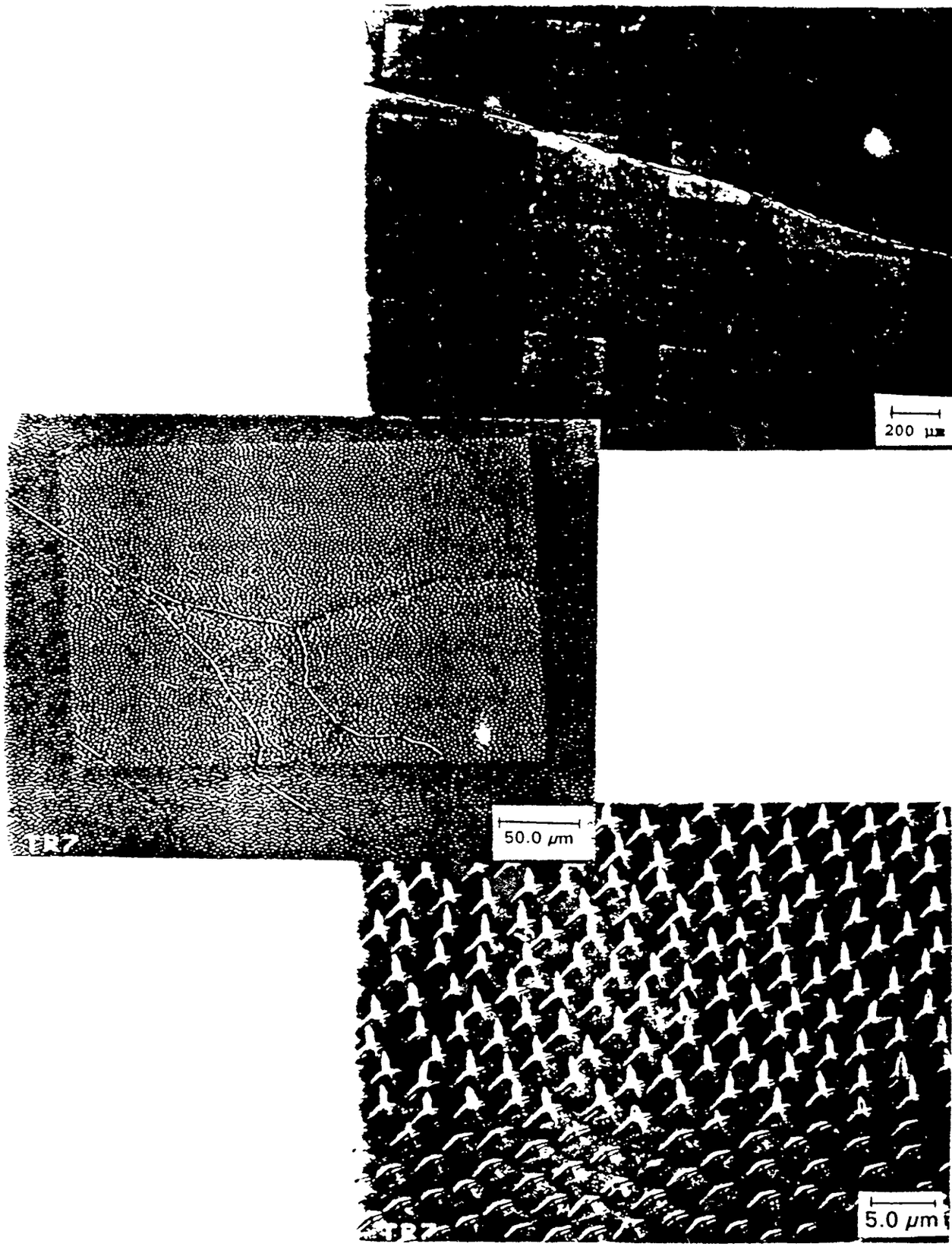

Figure A.3.4 Scanning Electron Micrographs of a Composite Sample Demonstrating Definition of Emitting Areas a) Pattern of Sixteen Emitting Areas; b) Detail of a Single Emitting Area, c) Detail of Edge of an Emitting Area.

The details of the processing developed to reach this step, and provide sharply pointed emitter tips via a plasma etching procedure, which represents a major step forward vis a vis earlier processes, has been described in an earlier section, and is not repeated here.

The process of fabrication of the grids involves deposition of molybdenum over the entire sample, subsequent to deposition of the insulating film (this procedure as presently performed is describe in another section of this report); spinning on of a resist layer; masking, exposure and development of the resist to leave the moly film in the intended grid areas protected; plasma etching of the moly to remove the film from the regions external to the emitting areas; and stripping of the resist to remove it from the now-defined grids and their connecting leads.

A comparable process is used to subsequently deposit gold on the connecting pads at the ends of the leads, which assures the ability to successfully beam lead electrical connections to the molybdenum grid films.

Development of the complete process flow is continuing, and still requires definition of the details of several aspects. The individual steps of the process are satisfactorily understood at this writing, and their integration into a usable process is not expected to encounter major difficulties.

Conclusions

A satisfactory process, which allows fabrication of precisely sized and located emitting areas, using photolithographic methods has been developed. This process sequence incorporates into a single step the procedures for defining the emitting areas, by removal of all emitter tips outside of the intended emitting areas, and the pointing of the emitter tips in their intended areas. This procedure is a unique plasma etching process

which has been successfully incorporated into the fabrication flow for the emitters.

Subsequent deposition of the insulating film and the grid is performed by physical vapor deposition as described elsewhere in this report, and then grid areas corresponding to the defined emitting areas are proscribed as discussed above using similar photolithography.

The process developed is capable of producing emitting areas of a wide range of sizes and configurations dependent only upon the design and fabrication of suitable masks. It is evident that this process has provided a capability for the Georgia Tech field emitter array cathodes which is comparable to any competing process, allowing complete freedom to fabricate arrays as required for a wide variety of potential applications. The maximum area of a single emitting area is limited by the maximum chip size available from the composite growth process. Significant progress has been made in increasing the typical chip size and further progress is expected.

Electron Beam Deposition Facility

In order to fabricate a low voltage field emitter array a number of thin film deposition steps are required. These include at least two molybdenum and one silica or alumina deposition. Specific to the fabrication of these arrays is a line of sight deposition process. Electron beam evaporation has been used previously, and has been shown to work very well in this application.

In order to accomplish the required depositions the system shown in Figure A.3.5 was constructed from individual components. The vacuum system was designed around a 1500 l/min diffusion pump that was backed by a 1400 l/min mechanical pump. In addition to acting as a forepump to the diffusion pump, the mechanical pump could be valved to rough pump the chamber during initial pump down. The diffusion pump is

topped by a liquid nitrogen cold trap which in turn is connected to a manual high vacuum gate valve which can be opened to bring the chamber pressure down.

The vacuum chamber itself consists of an 18 inch diameter by 18 inch tall pyrex collar mounted on an aluminum collar which has multiple vacuum feedthroughs around its circumference. Two of these feedthroughs are used for the electron beam gun high voltage connections. Another is connected to the electromagnet which is used to sweep the electron beam about the hearth. An ion gauge tube and a thermocouple gauge tube are connected to two others. One feedthrough is used for a quartz crystal monitor and another is connected to a Granville-Phillips precision leak valve. The top and the bottom of the pyrex collar are sealed by viton "L" gaskets. The top of the chamber consists of a one inch thick aluminum plate with vacuum feedthroughs placed at appropriate locations. A large feedthrough is centered in the top plate and is used to suspend the sample holder and heater assembly. The feedthrough supplies electrical connections for the sample heater as well as a thermocouple. The top plate is connected to an air cylinder which is used to raise the plate and make access to the inside of the chamber possible.

Inside the chamber is a SLOAN multihearth, 180° bent beam electron beam evaporation source. This source has four 3.2 cubic centimeter water cooled copper hearths. The source turret can be rotated by means of an external manual control so that up to four evaporation materials can be evaporated without breaking vacuum. The source is powered by a SLOAN model FIVE/TEN A power supply that is connected to a SLOAN Model MDC 9000 deposition controller. The deposition controller relies on a water cooled quartz crystal monitor which supplies information on deposition rate and accumulated film thickness. The crystal monitor, and deposition controller and the power supply combine to form a closed loop system which enables precise control of deposition rates

and film thicknesses. Because the deposition controller is microprocessor based and programmable, it controls start-up, soak power, deposition power, final film thickness and shut down completely automatically.

The SLOAN multihearth electron beam gun is equipped with an electromagnet which is used to sweep the electron beam along the length of the hearth. In addition, a rotating permanent magnet is situated so that the beam can also be swept across the hearth. This capability is critical when thermally insulating materials, such as alumina or silica, are deposited. By sweeping the electron beam across a larger area of the insulating charge a larger pool of molten material can be formed resulting in more stable deposition.

Previous results have shown that heating of the substrates is necessary to insure adequate adhesion of the thin films to the composite. A sample holder and heater assembly was constructed from a copper block and four 2 inch long x 0.125 inch diameter 100 watt cartridge heaters. The samples are easily held in intimate contact with the copper heater block by spring tension holders fabricated from W-Re wire. A type-K washer thermocouple is attached to the front surface of the sample holder and sees the same temperature environment as the samples mounted on the surface nearby. The heater power is provided by a Variac with the output controlled by a simple on-off proportional controller which is able to maintain the desired temperature within ± 2 to 3 degrees Celcius. A schematic view showing the spatial relationship between the e-beam hearth, the sample holder-heater assembly, the quartz thickness monitor and the low pressure oxygen source is given in Figure A.3.6.

Deposition Routine

The ZYW composite chips first come to the deposition facility after they have been screened for continuity and polished on both sides to a 0.25 μm surface finish. At this

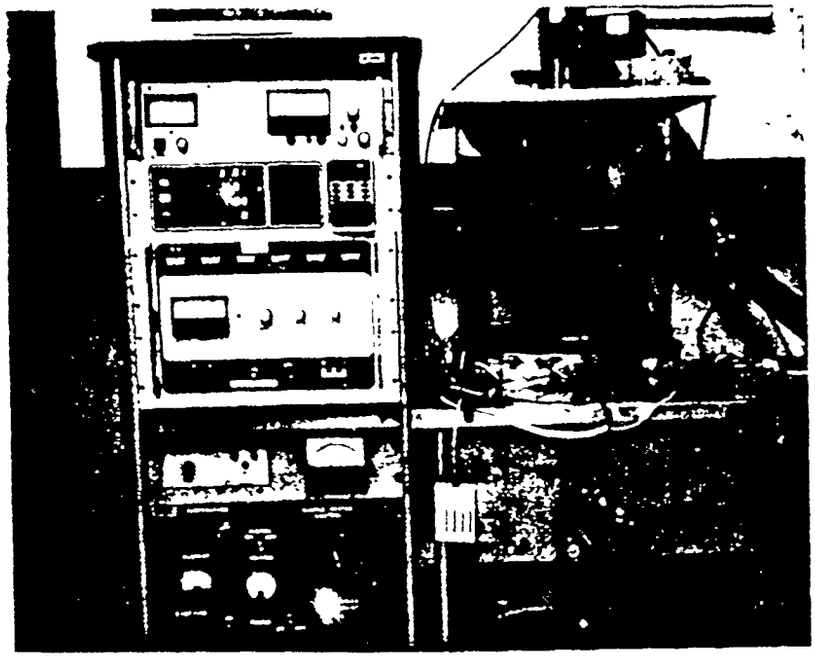

Figure A.3.5. Electron Beam Evaporation System Used to Form LVFE Structure.

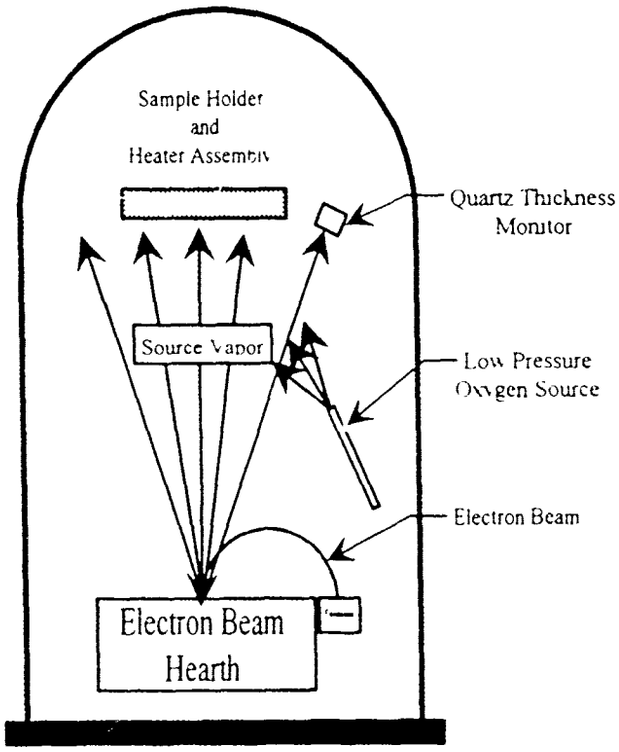

Figure A 3.6. Schematic of Electron-Beam Evaporation System, Showing the Location of the Heated Sample Holder Relative to the Hearth and Film Thickness Monitor.

point a molybdenum film is deposited on one side. This film serves two purposes. It provides protection to the back side of the chip during the etching step which exposes the tungsten fibers, and it acts as an electrode providing uniform electrical connection to the fibers during testing of the finished emitter arrays. The chips then undergo a number of processing steps before they come back to the deposition facility where the emitter structure is formed on the exposed active area.

Figure A.3.7 shows a schematic of the array structure displaying the relationship of each deposited layer. This figure also illustrates how the shadowing effect occurs during deposition and how it effects the finished geometry of the array. The procedure involved in depositing these films is outlined below.

Before the chips are mounted onto the sample holder they are vapor degreased in TCE. The sample holder is then installed, and heater and thermocouple leads are connected. The top plate is lowered and aligned so that the sample holder is directly above the electron beam evaportion source. Initially a movable shield is placed in front of the samples. It is subsequently moved out of the way once a constant deposition rate is verified by the quartz crystal monitor.

Once the chamber has been evacuated and the pressure is below $5x10^{-5}$ Torr the sample heater is started. The first deposition is typically silica which is deposited at 450°C. The heater is capable of heating the sample holder to this temperature in about 1 hour. After the silica deposition is finished the temperature is reduced to 300°C for the molybdenum deposition. This takes approximately an hour. The base pressure often increases by as much as an order of magnitude during the heating phase due to outgassing. Before beginning deposition the sample temperature is allowed to stabilize and the pressure allowed to drop to a maximum of $1x10^{-6}$ Torr. In order to insure that the silica

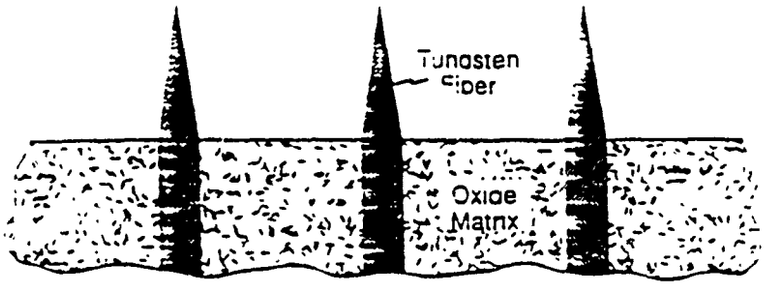

Step 1. Etch the polished composite wafer to produce free standing tungsten pins (emitters).

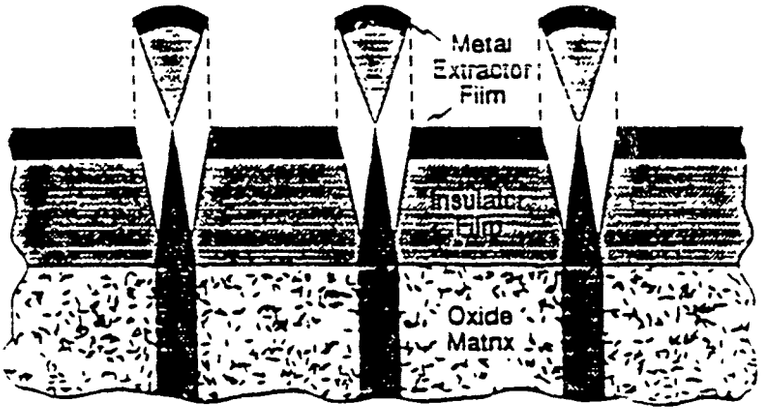

Step 2. Vapor deposit the insulator and extractor films, parallel to the fiber axes, to the desired thickness.

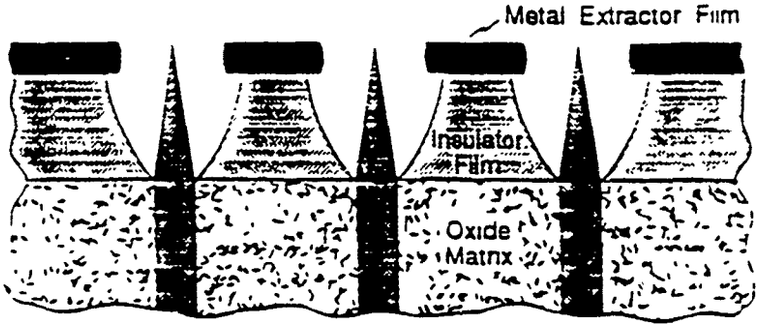

Steps 3 and 4 Remove the cathode cones ultrasonically and clean remanent oxide from the cathode tips using an acid etch.

Figure A.3.7. Schematic Diagram Illustrating the Deposition Sequence Used to Form the LVFE Structure.

film that is deposited is indeed an electrically insulating SiO_2 a partial pressure of oxygen is introduced into the system through the precision leak valve. The system pressure at the beginning of the silica deposition is typically $2x10^{-5}$ Torr.

The actual deposition of the films is very straight forward with the deposition controller being pre-programmed to ramp the power up to a soak power and hold it for an appropriate amount of time for each material to adequately outgas. After the preset soak time, the power is increased at a prescribed rate to that necessary to initiate evaporation of the material. When the evaporation rate stabilizes at either 2 Å/sec for silica or 5 Å/sec for molybdenum the shield is removed from in front of the samples. The film thickness is monitored so that the shield can be reinserted between the hearth and the samples when the desired thickness is reached. When the final film thickness is reached the deposition controller automatically drops the power back to a prescribed level or off.

After the silica deposition is completed the oxygen leak valve is closed and the system allowed to pump back down to a base pressure of not more than $1x10^{-6}$ Torr before the molybdenum film is deposited. This normally occurs while the substrate is cooling down to the molybdenum deposition temperature of 300°C. The thicknesses of the silica and the molybdenum films are programmed according to the average height of the exposed fibers for the particular group of samples being used. A total height is chosen so that the molybdenum extractor film is placed in the desired relationship relative to the tips of the fibers. For typical fibers of about 1.5 μm in height, the silica film is 1.0 μm in thickness and the molybdenum is 0.5 μm thick.

After processing is complete the sample heater is turned off and the samples are allowed to cool to room temperature in vacuo. This typically takes approximately 4 hours. When cool, the sample holder is disconnected from the heater leads and the

thermocouple and removed from the system. At this point the samples are removed from the holder and sent on to the post deposition processing where the cones are removed and the extractor grid is electropolished. Figure A.3.8 shows two views of an LVFE cathode as it appears after removal of the cones but prior to electropolishing.

A.4. Field Emitter Array Testing

DC Electrical Characterization

The system which has been assembled to perform DC IV characterization is illustrated schematically in Figure A.4.1. All measurements are performed in a stainless steel, cryopumped vacuum system (Figure A.4.2.) capable of a base pressure of about $5x10^{-9}$ torr. The system and the characterization process are described below.

The LVFE cathode specimen being characterized is mounted on a dual in-line pin chip carrier. The specimen's various isolated emitting regions and its extractor are connected to separate carrier pins. A collector positioned immediately above the emitting regions is also connected to a carrier pin. The carrier is plugged into a DIP socket electrically connected to a 20 pin vacuum feedthrough allowing external electrical connection to the specimen.

The vacuum feedthrough is connected via a multiwire cable to a computer system (Figure A.4.3.) through a switch box which allows selection of the individual emitting region. All of the electrical instruments communicate with, and are controlled by, a 386 personal computer equipped with National Instruments Lab Windows software and appropriate boards. A Quick Basic 4.5 computer program run within Lab Windows controls the data collection. This program allows the operator to preset the voltage range over which data collection is to occur, set the voltage increments, set the maximum

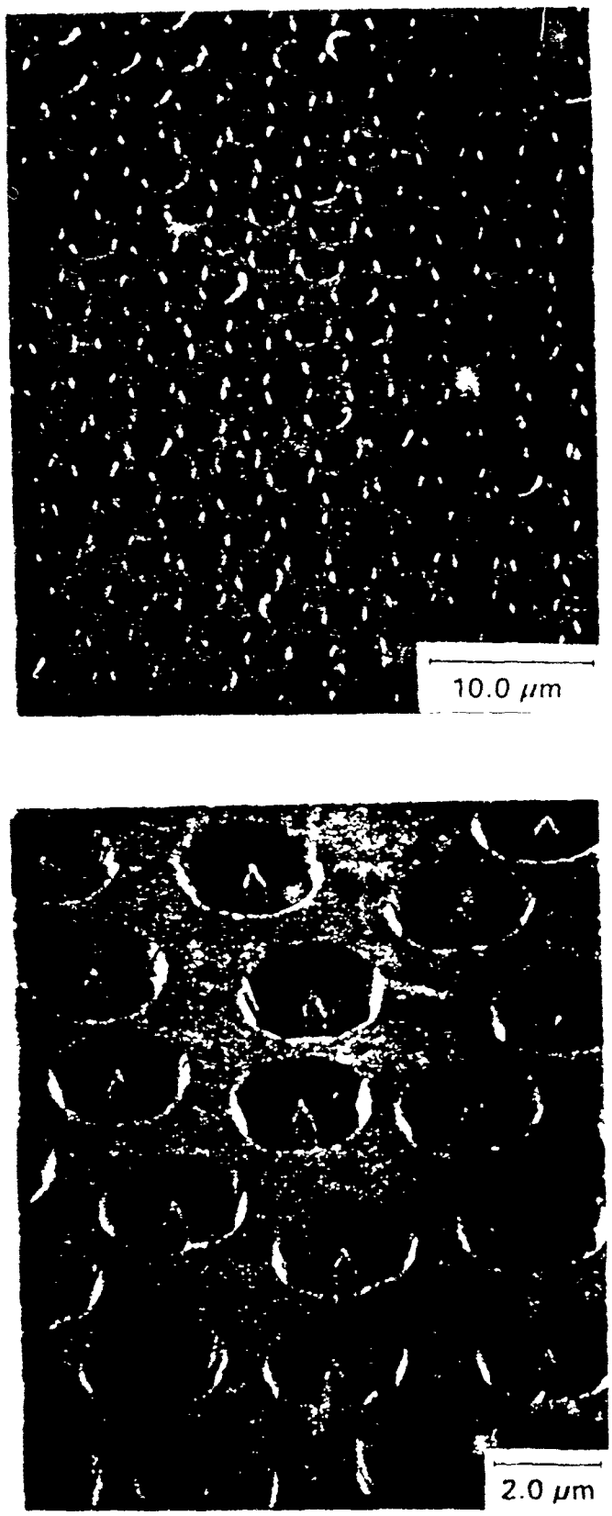

Figure A 3 8 Two Views of a LVFE Cathode After Removal of the Cathode Cones, Prior to the Electropolishing Step

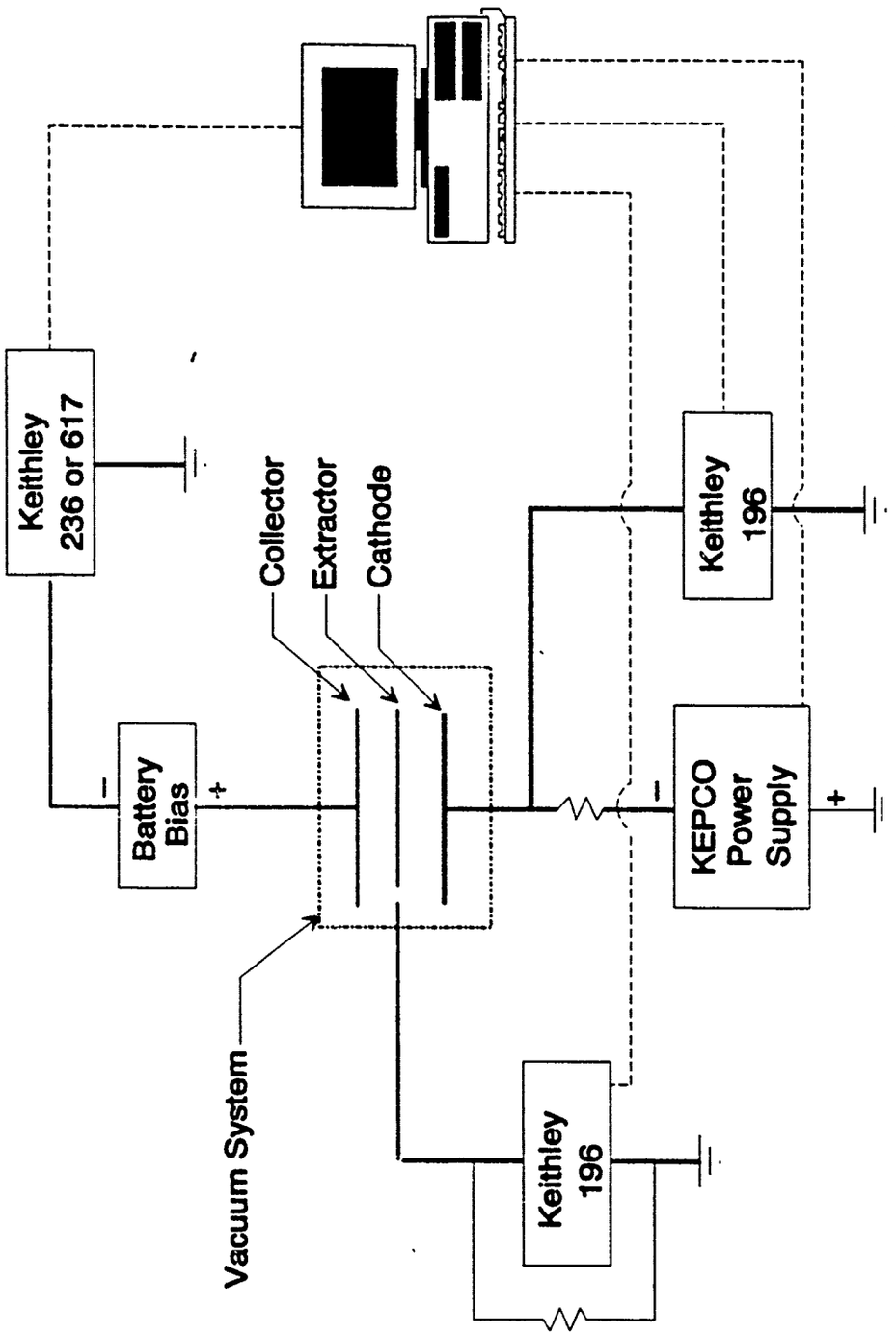

Figure A.4.1. Electrical Schematic Showing the System Assembled to Emission Test the LVFE Cathodes.

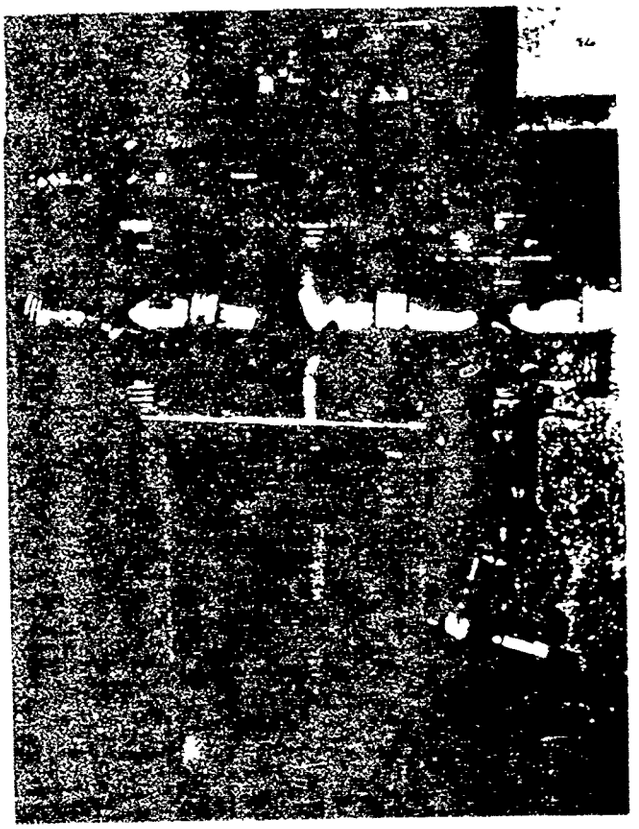

extractor voltage, and plots out the resulting IV curve, including the Fowler-Nordheim parameters.

An IV curve is generated by applying incremented voltages between ground and an individual emitting region (cathode) and measuring the resulting currents to the collector with an electrometer. The collector is biased positively to insure that it collects all of the emitted current. A voltmeter placed across the cathode power supply is used to monitor the cathode voltage. The current from the extractor to ground is measured by observing the voltage across a resistor placed between the extractor and ground. The measurements can be terminated if this current exceeds a preset value.

High Frequency Testing ($\leq$ 1 GHz)

Use of the DIP package used for DC testing as previously described is not satisfactory for RF evaluation, consequently a dual-in-line all-metal package supplied by Airpax is planned for use in this work. This package will also allow the mounting of samples up to 1cm in dimension, as opposed to the 6mm maximum size dimension usable with the DC package, providing a means to accommodate larger chip sizes as they become available.

Field Emission Microscope

Emission testing of a considerable number of LVFE cathodes has shown that pin-to-pin emission from the arrays is not uniform. Based on post mortem examination of failed cathodes, it is clear that some percentage of emitters in an array operate at sufficiently high levels that they eventually fail. Dynamically adsorbing and desorbing films on the surface of the emitters alter the work function of the tips. Consequently, the work function of the emitters in the array is assumed to be higher than the average value of 4.5 eV for a clean tungsten surface. Because the films are dynamic, the emission levels

change constantly at each pin tip as a function of time. Such behavior can readily be qualitatively observed in a field emission microscope. However, the magnitude of work function variation, and hence emission level, has never been quantified; nor is the stability of the surface adsorbates known.

Utilization of a field emission microscope, connected to a solid state camera-based imaging system, will yield quantitative information on emission from different tips in the array. Quantitative information will be obtained on the variation of emission from tip to tip, as well as the variation of emission from one tip as a function time. With this knowledge, information on the work function variation and film dynamics will be available to evaluate the effectiveness of different surface alteration techniques, such as ion implanted or CVD'd coatings.

To complement the work on the arrays, single tips will also be examined. From this series of tests information on the work function changes and the magnitude of those changes over the surface of the tip will be examined. This information should supplement the information obtained from arrays.

The experimental set-up is shown in Figure A.4.4. The system will be evacuated with an ion pump to vacuum levels in the 10^{-8}-10^{-9} torr range. An eight inch O.D. pneumatic gate valve with a 2.75 inch roughing port separates the ion pump from the test chamber. The test chamber will be initially evacuated to 10^{-4} torr range by means of a mechanical pump. Both a Bayard-Alpert ion gauge and a thermocouple gauge are mounted in the test chamber to monitor the vacuum level.

The cathode, whether an array or a single tip, will be mounted on a precision manipulator, set into a multiport flange with high voltage feedthroughs. The stage allows a 4 inch translation in the "z" direction in addition to "x" and "y" motion for cathode

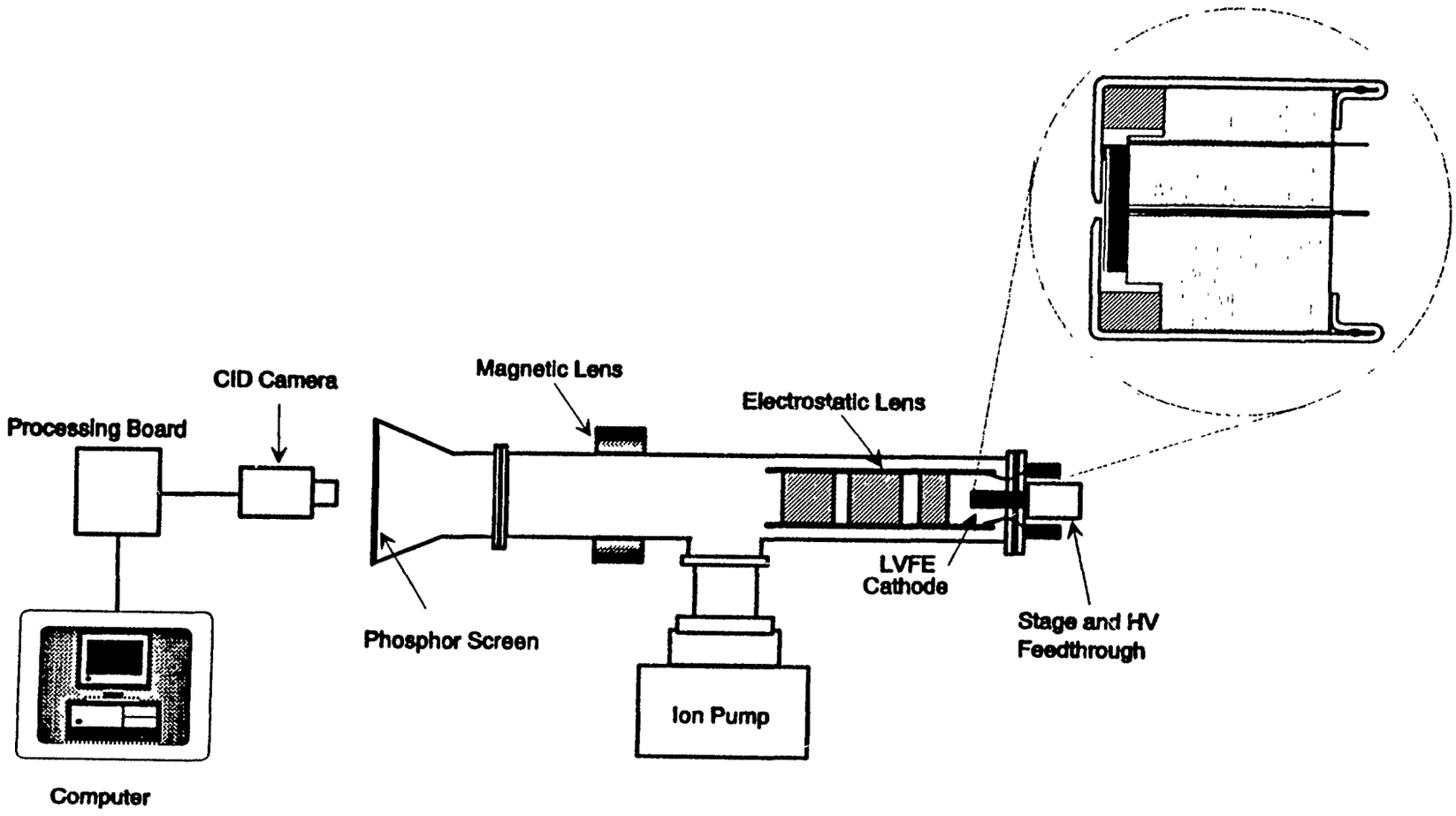

Figure A.4.4. Schematic of the Field Emission Microscope to be Used to Record Images of Operating LVFE Cathodes.

centering. The arrays tested will be 50 microns square consisting of approximately 100 pins. The cathode will be mounted in the G1 cup of a CRT gun assembly and is shown in the detail drawing in Figure A.4.4. The electron beam will be accelerated with a 10 kV potential, through a focusing system consisting of the CRT electrostatic lens assembly and a magnetic lens (CELCO model #B3041-7A) in order to focus the individual beams from each tip, onto a Type P37 phosphor screen. Type P37 phosphor, zinc sulfide:silver:nickel, was chosen for it's short extinction time (0.15 microseconds to 10% intensity) and for it's spectral response, which matches that of the solid state camera.

Impact of the emitted electrons on the phosphor screen will result in the emission of photons which will be detected by a CIDTec 2250D Charge Injected Device camera. The camera sensor consists of an array of 512 x 512 pixels and scans non-interlaced at 29.6 Hz. It will be focused such that the whole image on the phosphor screen is obtained and a shutter on the camera will allow "freeze frame" images to be captured. The output of the camera is available for analog recording on video tape or for digitization and subsequent analysis. "Freeze frame" images collected from the solid state sensor will be digitized into an 8-bit gray scale value by a Data Translation Model 2861 frame grabber/digitization board. The DT2861 has an on board memory buffer, allowing for up to eight images to be taken in quick succession if desired.

The system will be calibrated so that the gray scale level in the image can be associated with a known current density/current level and thus the emission from each tip may be monitored. Calibration of the apparatus will be accomplished by scanning a series of beams of known current densities from a CRT gun across the phosphor screen and recording the resulting gray levels in the digitization process. In this fashion the resolution and linearity of the phosphor screen and camera can also be determined.

Successive images in time will be taken to evaluate the emission characteristics and levels of individual tips in the array. The time intervals are yet to be determined, but the apparatus will be capable of obtaining an image approximately every 35 msec. Image analysis, such as subtraction, windowing and other pixel manipulation techniques, will be done to determine emission level variations from pin to pin, as well as temporal changes in the emission from a single pin. Since surface adsorbates are dynamic, time variations must be investigated to characterize the emission stability of the arrays and individual pins and to establish the duration of the existence of adsorbates and their effects on the emission.

III. FISCAL STATUS

Contract budget:	$568,572.00
Total expenditures through 28 February 93:	$443,827.09
Projected Expenditures 3/93 - 9/93:	$124,744.91